Chapter 3
Interaction of Particle Beams and Matter

Abstract This chapter teaches the basic understanding of the beam-matter interaction physics of photons, electrons, and ions relevant for accelerator applications. The two main parts of energy-loss and nuclear interactions will be discussed on the basis of examples and practically relevant quantities. The mathematics of depth-dependent reactions combines these two aspects resulting in a 1D model. Depth dependent reactions explain about 98% of the interaction physics of the typical fixed thick target geometry of applications resulting in reaction probabilities and equations for practical efficiency optimisation and device layout. A few examples of established codes and practical implementation of the knowledge concludes the chapter.

This section will discuss the physical basics for understanding accelerator applications. By far most of them rely on the interaction of the accelerated beam with some kind of target, may this be a sample, a production target or a human being. The four fundamental forces of physics represent the basis of all beam-matter interactions. From daily life we know gravity, a force extremely weak when normalized to the number of particles required per unit strength. Its range is large, but its small strength makes it negligible in accelerator applications. The electro-magnetic force has a similar range, but a significantly stronger effect than gravity. It keeps the world together by using photons to let positive and negative charges interact. In contrast to gravity it has two different charge polarities which we call plus and minus, leading to a possibility of shielding it via neutralisation of opposing fields. We already learned about its importance for accelerator applications with respect to the electro-magnetic technology required, but it also results many interactions of charged particles with targets such as stopping or elastic scattering. The strongest force, the strong force, also features the lowest range. It holds the nucleus together, but its range restricts to nuclear dimensions. It requires six charge types/flavours usually named red, green, blue, and their anti-counterparts and is mediated by gluons. This force draws responsible for inelastic scattering in the form of fission and fusion reactions, allowing us to change the atomic nucleus, if we are able to bring two particles into their strong force range. Its strength draws responsible for the large specific energy content of nuclear fuels, exceeding the one of chemical (= electro-magnetically bound) fuels by about 10^6. Lastly, the so-called weak force is responsible for most radioactive decays and

S. Möller, *Accelerator Technology*, Particle Acceleration and Detection,
https://doi.org/10.1007/978-3-030-62308-1_3

neutrino interactions. Its mediators, the W and Z bosons are heavy, leading to a low range in the order of the atomic nucleus. Its weakness manifests in the extremely low interaction probability of neutrinos, which only interact via the weak force with matter (see later in Sect. 4.4).

In contrast to the typical situation in fundamental particle physics, where two beams counter-propagate and collide with each other in an interaction zone (fixed centre-of-mass), application targets consists of normal stationary matter (fixed target). Furthermore, the target comprises several different species, at least electrons and a set of more or less abundant elements (desired and impurities) leading to complex interactions. Besides this, also the kinematics and the chain of events of the interaction differ between colliding beam and fixed target situations.

The Rutherford experiment marks the original fixed target experiment, featuring already many of the physical aspects still relevant in accelerator applications today. Rutherford wanted to understand the nature of the atomic nucleus and its charge distribution. At that time, over 100 years ago, it was not quite clear whether the nucleus is a compact object or a cloud of positive charges mixed with a cloud of negative electron charges in the atom, since both would result in a neutral atom as seen from the outside. Rutherford wanted to falsify one of the models by a scattering experiment of an ion beam with a fixed target. Firstly, he calculated the kinematics and scattering probabilities (cross-sections) for each situation, yielding the famous Rutherford formula (3.1). With this knowledge, he designed an experiment for shooting some MeV α-particles (doubly ionised helium: $^4He^{++}$) from a nuclear decay through a thin gold foil with particle detectors around it. The experiment yielded an angular probability distribution of the scattered particles according to the compact nucleus model represented by his formula, constituting the current understanding of the atomic structure. In his experiment, Rutherford was lucky, because with the technology of his time he was already able to produce a foil thin enough (some 100 nm) to be passed by 5 MeV alpha particles, which was the maximum he was able to provide. We will see in the following sections that α-particles of that energy not even pass 10 μm of gold (assuming surrounding UHV) and hence the technological aspects were a key parameter in the success of Rutherford's ground-breaking experiment.

$$\frac{\mathrm{d}\sigma_R}{\mathrm{d}\Omega}(E) = \left(\frac{Z_1 Z_2 e^2}{4E_0}\right)^2 * \frac{1}{\sin^4(\theta/2)} \tag{3.1}$$

Each interaction has two sides, on the one hand its probability of occurrence called the cross-section (which was Rutherford's testing ground) and on the other hand the collision process of each individual instance of this reaction called the kinematics. To change from the view of the probability/cross-sections to the process/kinematics, we first define the situation. We call the accelerated particle shot into the situation the projectile. Definitely the projectile starts the situation, since it is initially the only moving particle (remember we are talking about fixed target situations). Please note this view is from the laboratory system, in the centre-of-mass system all particles are moving also in a fixed target reaction. The projectile of mass m_1 hits the target of

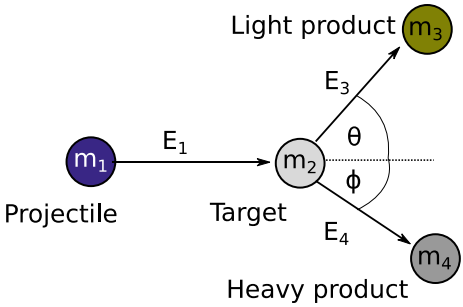

Fig. 3.1 Kinematics of a 2-body reaction with a stationary target in the laboratory frame (E_2= 0) has 9 parameters. The energies and angles of all particles have unique relations defined by mathematics. In contrast, a reaction with more products (n-body reaction) also conserves energy and momentum, but allows for more than one solution as will be explained later

mass m_2 with kinetic energy E_1. Both particles scatter and emit a light product m_3 and a heavy product m_4, each having a certain emission angle (Θ and ϕ) against the initial vector of the projectile. In 3D Θ and ϕ will describe circles when seen from the projectile movement direction due to the rotational symmetry of the process. The whole situation is depicted in Fig. 3.1.

This so-called two-body reaction is the standard situation we have to consider in accelerator applications. Single reactions with more than two input particles require extreme densities. Those conditions are technologically so far inaccessible or of minor importance and will not be considered in this edition (maybe in future ones). Reactions with more than two output particles commonly appear in nuclear decays, in particular β-decays feature 3 output particles (electrons for β^-, positrons for β^+, neutrinos and a heavy nucleus, see Chap. 5), and nuclear reactions can feature 3 (E_1 $>\approx$ 10 MeV) or more products with increasing projectile energy. These reactions add the complication of interconnected spectra for all outgoing particle properties, in contrast to the kinematics of the two-body reaction featuring only a single solution at each product angle. In any case, the whole situation has to fulfil momentum and energy conservation, which allows calculating the respective product parameters with the knowledge about the four masses and, in the case of two-body reactions, any four other parameters of the situation (leaving 1 unknown + 1 equation = unambiguous solution), see Sect. 3.3.2. The mathematical flexibility implied by these equations forms an important aspect of our physical understanding and also technological exploitation of beam-matter interactions. As we will see in the course of this chapter, everything interacts with everything, even with the vacuum, but the mathematical formulations allows us tailoring and identifying the reactions. This additional information compensates for the lack of information provided by detectors (Sect. 2.5). The same equations apply for material analysis, isotope production, or patient treatment, just with different unknowns in the equation system.

The interaction of beams and matter covers a wide range of specific physics. Not all of them are fully or even partially understood. In view of applications we

divide the level of knowledge into three categories: Theoretical, semi-empirical, and empirical understanding. Full theoretical models requiring no external input, except for fundamental constants, so-called ab initio models, are the highest level of understanding. Think of a treasure quest. Theoretical understanding equals a situation where you have a full map containing all the information on what the treasure looks like, how much gold it contains, and the mm resolved path this would allow walking to the treasure blind with only your feet (or technology) limiting the amount of success. If you know there is a treasure somewhere, but you only have a plain path drawn on a handkerchief, without coordinates, scales, or the like you have a semi-empirical understanding. It tells you which turns to take and the dangers lurking on your path, but you do not know where to start or how long the way will be and which dangers wait on your path. The same applies for beam matter interaction. Some cross-sections, such as Rutherford's, were understood to their fundamental physics and a theory was found accurately describing them. Others have been investigated deeply and mathematical relations were found empirically, but certain constants, factors, or limiting cases cannot be covered by existing semi-empirical models. A few cases, such as the radioactive decay, were broadly investigated experimentally, but due to the lack of understanding no type of extra- or interpolation of data is possible. In this lowest level of understanding we only have an empirical qualitative estimate of the order of magnitude and the influence factors of the process, but we do not even know if this covers the full space of possible pathways of the process.

Rutherford understood the nature of the target structure in his gold foil experiment by the match of the cross-section calculated from his hard sphere model and the agreements with the experimental results. Interestingly, most of the α-particles actually passed the gold foil in Rutherford's experiment undisturbed. We can quantify the interaction probability w using (3.2) and the gold atomic density ρ by multiplying with the Rutherford cross-section σ and the foils thickness d.

$$w = \sigma(E) * \rho * d \tag{3.2}$$

The interaction probability remains in the percent range, even if we infinitely increase the gold foil thickness beyond Rutherford's thin foil. From common sense, but also from a mathematical limit consideration, it becomes obvious we didn't completely understand the situation: An infinite target thickness should yield a 100% reaction probability for each projectile, otherwise they would fly through the target, a situation empirically non-existent. By increasing the foil thickness beyond 10 μm we would come to know that the α-particles will already get stuck in the foil way before Rutherford's reaction probability even has a chance reaching 100%. Therefore, at least a second mechanism stopping the α-particles has to exist besides Rutherford-scattering. The question arises which interactions were missing in Rutherford's description, since a particle beam will not stop by itself, just like a spaceship will not stop by itself in the vacuum of the universe.

So far we skipped considering 98.7% of the particles in the gold foil, the electrons attached to the gold nuclei forming the atom. Gold has 79 times more electrons than nuclei (= nuclear charge Z), which can undergo the same 2-body reactions with the

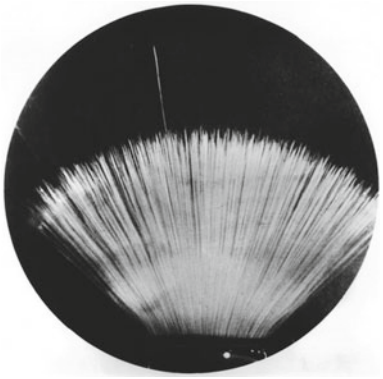

Fig. 3.2 An α-particle source (≈ 5 MeV α) placed at the bottom emits α's into a cloud chamber. The bright tracks indicate individual particle tracks. The particle range in the cloud chamber's alcohol mixture slightly differs for each particle due to statistical effects of the stopping, even a 50% longer spike is present. Reprinted from physicsopenlab.org CC-BY 4.0 license

projectiles as the nucleus, although with different kinematic parameters. Everything relies on the ratios of the interaction cross-sections and the results of the interaction. There are actually significant amounts of interactions with the electrons contained in the gold foil, but due to the strong mass difference of electrons and α-particles the energy transfer remains small in each interaction. In a reasonable approximation, the electrons act like an aether continuously slowing down the α-particles or, in general, charged particles, passing through them. Imagine it like walking through IKEA's Småland ball pool with the force required to push away the balls from your way slowing you down. The ratio of ball to human mass even approximately resembles the electron to α-particle mass.

Rutherford's experiment was designed in a way to minimize this slowing effect by staying in the limit of a thin target. Upon increasing the foil thickness we slowly leave the *thin target* regime and the energy-loss of the α-particles becomes visible/measureable. At a gold foil thickness of about 10 μm all α-particles will stop inside the foil and Rutherfords experiment would not yield any measurable quantity in the forward direction. In the backward direction the situation will also change, as the reactions from different depth will add up. The thickness related to this so-called *thick target* limit strongly depends on the beam and target properties. The situation gets nicely visualized in a cloud chamber in Fig. 3.2 with no α-particle reaching the top end of the cloud chamber.

Particle beams do not see distance when passing through matter. Of course, for the beam optical aspects of divergence and direction remain relevant as demonstrated in Fig. 3.2, but here we focus on the beam-matter interaction since the distances are relatively short (e.g. the 10 μm foil). In order to understand the way particle beams see matter let us consider the following three situations: A beam gets fired onto a solid metal, the same metal but as a metal foam with vacuum in the pores, and, last but not least, the same metal foam but with air inside the pores. The situations are

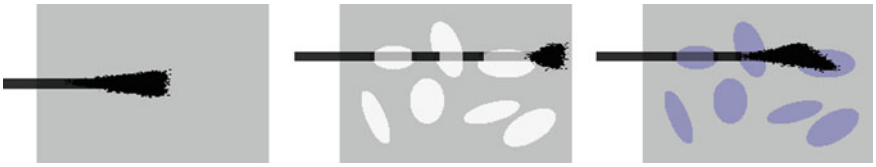

Fig. 3.3 Illustration of a beam (black line) in a solid (grey), a porous solid with vacuum inside the pores, and one with gas inside the pores. At the end of its range, the beam spreads out due to the statistical nature of scattering. In its interactions, a beam only sees matter, not distances. In vacuum, the beam travels undisturbed, like a space ship. In matter, the intensity of interaction depends on the matter density, hence gas volumes show lower interaction rates than solids

depicted in Fig. 3.3. In the first case, the beam travels a depth X into the material until its energy is dissipated. In the porous material the beam will lose energy when passing the metal, but in the pore's vacuum no energy is lost, hence the total range extends by the porosity aspect. In the third case, the pores also contain matter (gas), but the relatively low density of gas yields only a very small influence. The range in the pore exceeds the range in the metal, but gas still contributes to the energy-loss. Section 3.2 discusses the quantification of the beam stopping and its mathematical treatment.

Usually the projectile (photon, electrons, ions) beams density is insufficient for simultaneous reactions of several projectiles with single targets and reactions between projectiles are negligible due to the low relative speeds (= low emittance). Also target densities of normal matter are too low for reactions with multiple targets. This allows treating each beam particle individually in the so-called binary collision approximation (BCA). Therefore, the interaction of a beam with a target equals the sum over all the independent individual reactions. The BCA constitutes an important basis for our understanding and quantitative computer modelling of beam-matter interaction. This may sound trivial, but the exchangeability between the individual particle and the ensemble (beam) picture will become an important tool for understanding and mathematical treatment of beam-matter interactions.

In order to understand and work with something you have to give it a name. In addition to these energy-transfer reactions nuclear reactions become possible at higher projectile energies. Naming of nuclear reactions follows international conventions. The naming needs to include the target, projectile, and products. The reaction of a ^{12}C target with a ^{3}He projectile resulting in a proton and a ^{14}N product reads for example ^{12}C(^{3}He, p)^{14}N. For describing a class of reactions or shortening the naming, the same reaction could also be named (^{3}He, p) corresponding to a naming scheme (projectile, light product). (p,n) describes a typical reaction with two products, a 2-body reaction. Correspondingly (p,2n) and (p,n+^{4}He) describe reactions with three products, (p,3n) with four products and so on. If we want to describe a class of reactions, leading for example to the same element, we can introduce a variable x in the form (p,xn) with $x = 1$ to infinity to discuss reactions producing only neutrons.

3.1 Absorption and Reactions of Photons

We first take a step back away from the massive (mass > 0) charged particles produced in accelerators in order to improve our understanding of the interaction of particle beams with matter. Mass-free (or more correctly rest-mass-free) particles like photons necessarily have to travel with the speed of light, hence they cannot be slowed down. Logically for these particles, an energy-loss mechanism by friction is not possible, but energy can only be transferred via a reduction in quantity or intensity, respectively. This directly leads to a differential equation with an exponential decay solution of the photon beam intensity I in depending on the distance d passed in matter, equivalent to a constant absorption probability for each individual photon per passed matter particle.

$$\frac{I}{I_0} = e^{-d\mu} \tag{3.3}$$

Due to the lack of the friction mechanism, photons typically achieve the longest attenuation length μ and hence range (distance d) for a given kinetic energy of the considered species (e^-, ions, neutrons). The attenuation length increases with increasing photon energy. We already saw the technical effect of this fundamental physics in the detector Sect. 2.5 in Fig. 2.44 with the required detector thicknesses being largest for photon absorption. Also in radiation protection, Sect. 2.7.3, this and the exponential decay law lead to thick shielding requirements for photons.

Having said photon beams only lose energy by a reduction of intensity is actually not entirely accurate. For lower energies, scattering dominates the interaction of photons and matter. Scattered photons are absorbed and instantly reemitted in a different direction and hence cannot be considered as the same particle or part of the same beam population. A set of mechanisms exists for the interaction of photons with electrons. Scattering processes (approximately) conserving the photon energy dominate the photon matter interaction for lower energies up to the binding energies of electrons to atoms (e.g. 13.6 eV for H). This class of elastic process retains coherence (= phase relation) with the original beam. A prominent example among this is the Rayleigh scattering which leads to the blue sky, since the processes cross-section is inversely proportional to the fourth power of the wavelength, scattering more blue than red or green light in the observer's direction. With increasing photon energies or shorter wavelength, respectively, the elastic scattering energy transfer increases. With sufficient energy transfer, remember our scattering partner binds to atoms, the electrons gain enough energy to leave their binding state. Starting with this energy, the elastic scattering becomes incoherent, since the electron receives part of the energy. This so-called Compton scattering follows a probability distribution given by a cross-section called the Klein-Nishina formula, (3.4).

$$\frac{\mathrm{d}\sigma}{\mathrm{d}\Omega} = \frac{1}{2}\left(\frac{Z^2e^2}{4\pi m}\frac{E'}{E}\right)^2\left[\frac{E'}{E} + \frac{E}{E'} - \sin^2(\theta)\right] \tag{3.4}$$

This differential cross-section describes photon scattering from free resting point charges (electrons or ions), a situation only approximately true for electrons in atoms, with mass m, charge Ze, and the scattering angle Θ between incoming (energy E) and outgoing photon (energy E'). This formula only approximately describes the situation, but allows understanding the basic trends with an analytical description. The scattering cross-section decreases with the photon energy, hence Compton scattering becomes less efficient for high energy photons. The cross-section also decreases with increasing energy transfer and scattering angle. For photon energies small compared to the electron rest-mass $m_e c^2$ only negligible energy transfer occurs; the low energy limit of Compton scattering yields the coherent elastic scattering process discussed above. In all cases, (3.4) leads to a continuum of scattered photon energies, similar to Bremsstrahlung where electrons penetrate matter.

In parallel to the incoherent scattering Einstein's photoelectric-effect, the ionisation of atoms or the freeing of bound electrons, respectively, takes place. Equation (3.5) describes the cross-section of this inelastic process. It requires photon energies above the binding energy of the electrons to their atoms. Energy in excess of the binding energy will end up as kinetic energy of the released electron. All atoms above hydrogen (H) feature several electrons, each with different binding energies. The ionisation of the electrons from the innermost shell, called the K-shell, requires the highest energy in the order of a few 10 keV for heavy elements. The higher a binding level in the atomic shell, the lower its binding energy due to the core charge shielding of the inner electrons. Each binding state represents an independent instance of the photoelectric-effect, leading to so-called absorption edges at the given binding energies.

$$\frac{\mathrm{d}\sigma}{\mathrm{d}\Omega} = \text{Constant} * Z^5 * E^{-3.5} \tag{3.5}$$

The free spot of the released electron will quickly be reoccupied by another electron. The involved binding energy remains the same, but now has to be released in the form of a photon. In particular for the inner binding shells, also bound electrons from other higher shells can reoccupy the free position. These inner conversions emit photons with an energy given by the difference between initial and final binding state. A table of possible conversions arises, from which the innermost shells (K and L) are given in Fig. 3.4. The absorption of photons with an energy equal to the binding energy or higher can only lead to a complete release of the electron. The process can be triggered not only by photons, but also by charged particles as we will see later.

At the highest photon energies, new inelastic scattering processes add up to the interaction list. Up to here all photon interactions involved scattering with more or less free electrons. The quantum nature of the bindings implies certain specific energy limits. With photon energies above 1022 keV a new interaction process with the nucleus becomes possible. This interaction converts the photon energy to matter/mass. All physical processes have to conserve energy, momentum and quantum numbers. Consequently, for producing massive particles only matter antimatter pairs can be produced. With a rest-mass of 511 keV/c^2, 1022 keV and more

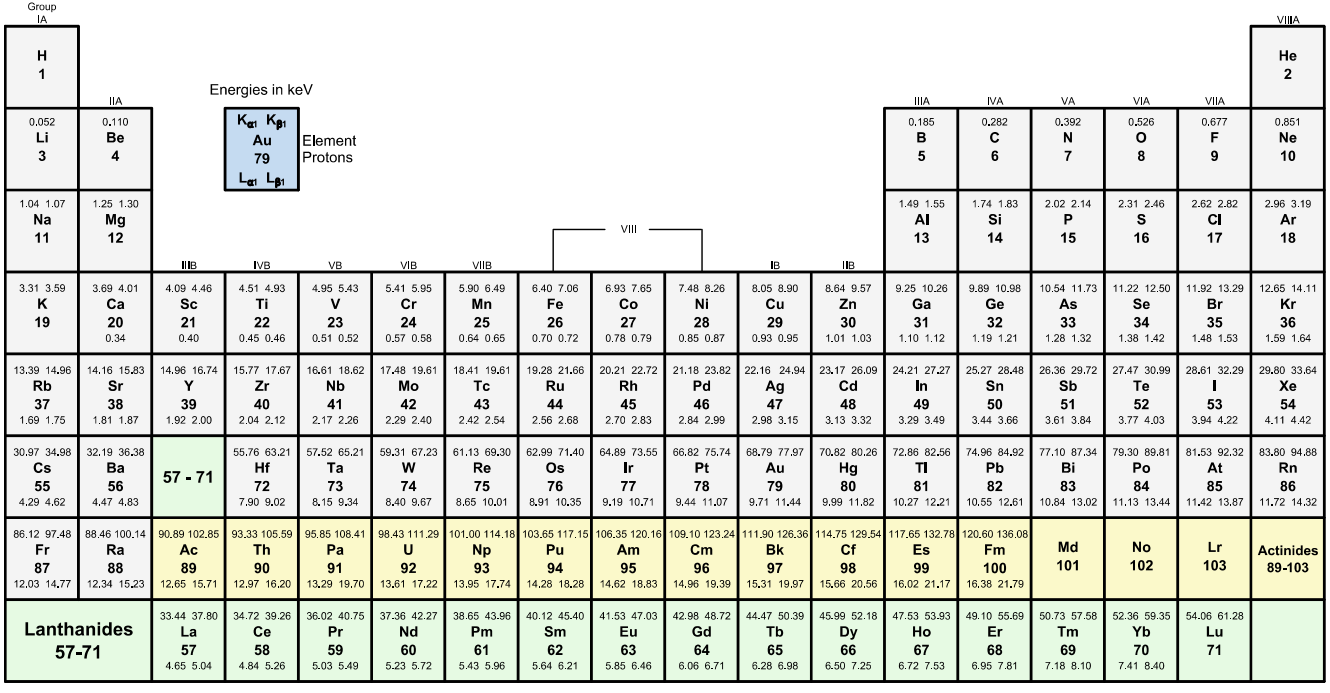

Fig. 3.4 Chart of the first four X-ray absorption/emission energies along the periodic table of elements. Generally emission and absorption of photons are connected in physics, hence all of these energies relate to absorption edge for photons passing through the elements and also emission lines when exciting the atoms via particle beams

allows for the production of electron-positron pairs. The process requires a nucleus to balance the momentum. Balancing the momentum with an electron requires slightly higher energy due to decreasing momentum per energy for lighter particles (= same amount of momentum transfer requires more energy transfer), favouring a nucleus as partner. Positrons being the anti-matter equivalent of the electron cannot survive in normal matter, quickly leading to the emission of two 511 keV photons from the annihilation of the positron with a random electron (the reverse process). At even higher energies, a disintegration of nuclei, so-called photo-nuclear reactions, becomes possible, releasing neutrons and other heavy particles.

In the accelerator application context, typically photon energies are between 1 keV and 10 MeV. Plotting a graph of all the discussed processes demonstrates the diversity of effects of photons in matter, see Fig. 3.5. The underlying data are well documented for the whole periodic table and are available online e.g. from the XCOM database (Berger et al. 2010). The sum of all processes leads to a mostly exponential decrease of attenuation with photon energy up to 1 MeV, from where on it stays constant. We have seen all processes tend to break down photon energy to smaller and smaller chunks. Some of these chunks have discrete energies due to quantum effects and some continuum distributions. For example the high energy processes convert a 2000 keV photon to an electron-positron pair with some kinetic energy. The particles annihilate to two 511 keV photons, which could then most probably Compton scatter to photons

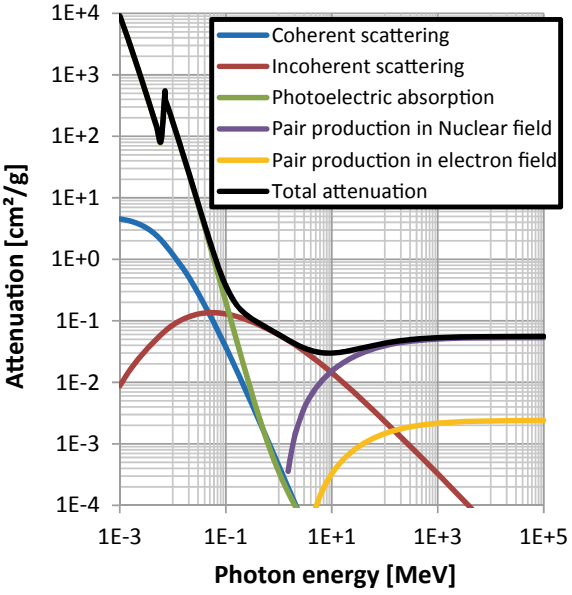

Fig. 3.5 Photon energy dependence of the different reaction channels of photons with iron. At 7.06 keV the K edge of iron leads to a sudden increase in attenuation, compare Fig. 3.4. The attenuation multiplied with the material density yields the exponential fall-off length μ, (3.3). Data from NIST XCOM Database (Berger et al. 2010)

and electrons of even lower energy, which then induce photoelectric electrons and photons, and so on. This kind of salami tactics consumes higher energy photons in a chain of events with many secondary particles involved finally ending up at particles with negligible energy.

Accelerators cannot directly influence or produce photons, but they arise from several processes of accelerated charged particles as secondary particles. We already came to know the Bremsstrahlung and synchrotron radiation, which describe spectra of photons produced by deceleration of charged particles, e.g. when passing matter. The decay of radioactive inventory and numerous nuclear reactions represents the second relevant source of high energy photons. These photons originate from the atomic nucleus and were given the name gamma-ray (γ) in contrast to X-rays originating from the atomic electron shell. Therefore, in the accelerator context photons potentially represent a problem, since they contribute to the radiation dose rates, but originate from fundamental processes. On the other hand many applications rely on using the production of photons. For example, the interaction of charged particles with bound electrons produces known photon energies, Fig. 3.4, allowing for elemental identification.

3.2 Range and Stopping of Charged Particles

Beams of massive charged particles (electrons, ions) follow different physics than photons, as their number is conserved by fundamental laws (like the conservation of velocity for photons), but their velocity is variable. For deep insight into the physics and mathematics of particle beam stopping and interaction with matter the reader is referred in particular to the book (Sigmund 2006) and also the accompanying book to the famous ion stopping software SRIM (Stopping and Range of Ions in Matter) which includes many examples and numbers of ion stopping (Ziegler et al. 2008).

Stopping of charged particles predominantly arises from the interaction of the beam with the electrons in matter (IKEA's Småland ball pool friction effect), similar to photons. The terms stopping, stopping power, specific energy loss, dE/dx, and friction are used more or less as synonyms describing an effect of an energy loss per length (e.g. MeV/mm), normalised to mass density (e.g. MeV cm^2/g), or per passed atoms [e.g. keV/(10^{15} atoms/cm^2)]. In fact, since the collisions with electrons induce stopping, distances cannot play a role for energy loss (as discussed in Fig. 3.3), making the energy lost per passed atom/area the most fundamental quantity. The Bethe-Bloch formula (3.6) for stopping power S in energy E lost per travelled length x describes this for ions in matter. Stopping depends on ion velocity not energy, but energy is usually the interesting quantity for other aspects of beam-matter interaction.

$$S_B(E) \equiv \frac{\mathrm{d}E}{\mathrm{d}x} = -\frac{n_e z^2 e^4}{4\pi m_e v^2 \epsilon_0^2}\left(\ln\left(\frac{2m_e v^2}{I\left(1-\frac{v^2}{c^2}\right)}\right) - \frac{v^2}{c^2}\right) \tag{3.6}$$

With electron density n_e of the material, projectile elemental charges z (e.g. $z = 1$ for electrons and hydrogen ions), projectile velocity v, a mean excitation energy of the target material $I(\approx 10\,\text{eV})$, and m_e, ε_0, c, and e fundamental constants. At energies below a few 100 keV/amu (atomic mass unit) ions additionally lose relevant amounts of energy due to collisions with nuclei (the billiard table effect). This nuclear aspect of stopping transfers energy to the target nuclei leading to cascades where individual particles hit nuclei and transfer enough energy for the hit nucleus to hit further nuclei, see Sect. 7.4.

Electrons also lose energy due to collisions with target electrons, but with their correspondingly higher velocity at a given energy the relevance of several effects changes. Relativistic effects and Bremsstrahlung reach a relevant level at significantly lower energy compared to ions. In particular ions have to be beyond our considered energy range of 250 MeV for this, while electrons require only about 1 MeV. The Berger-Seltzer-Formula describes the stopping power of electrons consisting of the collisional and the Bremsstrahlung part. Bremsstrahlung dominates the energy-loss of electrons for example above 10 MeV for Pb or 400 MeV for H targets:

$$S_E(x) = \frac{e^4 n_e}{8\pi\epsilon_0^2 m_e c^2} * \frac{1}{1 - \frac{1}{\gamma^2}} * \left[\ln\left(\frac{2(\gamma + 1)}{\left(I m_e c^2\right)^2} \right) + F \right] \tag{3.7}$$

Equation (3.7) follows a different trend with similar input parameters and the Lorentz factor γ as a measure for the electron energy. The function F adds a term which depends on the target material properties and the electron velocity, typically small in the energy range considered here. Figure 3.6 compares the total stopping powers of electrons and ions. The behaviour for different ions is similar with a clear maximum in stopping power around a few 100 keV/amu and a minimum in the GeV range. Electrons in contrast have a minimum at around 1 MeV with higher values for

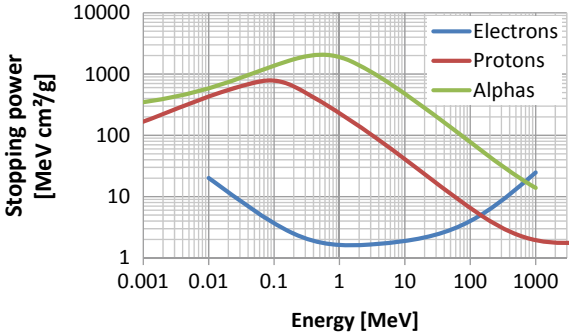

Fig. 3.6 Stopping power of charge particles in carbon. The stopping per length is calculated by multiplication of the values with the material density. Up to about 100 MeV the stopping power of electrons is about 100 times smaller compared to ions. Furthermore electrons show a different behavior, while different ions have similar but shifted stopping functions. Data from National Institute of Standards and Technology (2019)

small and large energies. In all cases, we see the graphs do not strictly follow (3.6) and (3.7) in particular in the low energy half. The equations describe an important part of physics, but additional higher order effects add up to the collisional stopping in the high and low energy limits.

Unfortunately, physics becomes very complicated in particular at lower energies. The electrons in the solid also move with the so-called Fermi velocity, changing their stopping effect if the projectiles have comparable velocity. Electrons on the other hand suffer additional energy losses by Bremsstrahlung emitted due to their strong deceleration in matter above a few MeV. We will not discuss the details of these higher order corrections in detail, but refer the reader to the given literature mentioned earlier. To summarise the findings: In particular at low energies stopping cannot be completely described analytically, but rather semi-empirically with fits to experimental data. This implies a limited accuracy in these energy ranges, compared to a full theoretical understanding. Uncertainties of the best known stopping powers range up to 6% (Ziegler et al. 2008), with the accuracy of full stopping models improving towards 1–2% at a few MeV/amu (the sweet spot).

For calculating the stopping S_{Mix} of elemental mixtures such as stainless steel or human skin, Bragg's rule applies. Within this rule, the total stopping power is given by the atomic fraction ρ_i of the weighted sum over the individual stopping powers S_i of each pure element, (3.8). Deviations from Bragg's rule occur in materials with strong chemical interactions between their constituents, in particular with light elements. While deviations <2% occur for metals and heavy elements, a value of 6% was found e.g. for SiO_2 and H_2O and values up to 20% for other special cases. Due to the practically infinite number of compounds, only a few common compounds were experimentally investigated for the correction factor. Some of them are available in the SRIM code (Ziegler et al. 2008).

$$S_{\mathrm{Mix}} = \sum S_i * \rho_i \tag{3.8}$$

The stopping power translates to a particle range. After this range the projectile has lost its energy and neutralizes with the target. In particular with ion projectiles shot into solids, this process is called implantation. The variations in stopping power lead to a typical energy deposition curve for ions. This so-called Bragg-curve, shown exemplary in Fig. 3.7, not only tells us the average depth of implantation of ions, but also demonstrates the strongly inhomogeneous deposition of collisional damage and beam power with its peak. This inhomogeneity increases with ion beam energy for energies above the stopping power maximum due to the monotonous decrease of stopping power with increasing energy, see Fig. 3.6. For technical materials the Bragg peak induces thermo-mechanical problems due to the combination of collisional damage, maximum power deposition, and implantation of ions. The particle range x calculates by integrating the stopping power S of the target of density ρ_S from the primary beam energy E_0 (= projectile energy E_1) till zero beam energy according to (3.9).

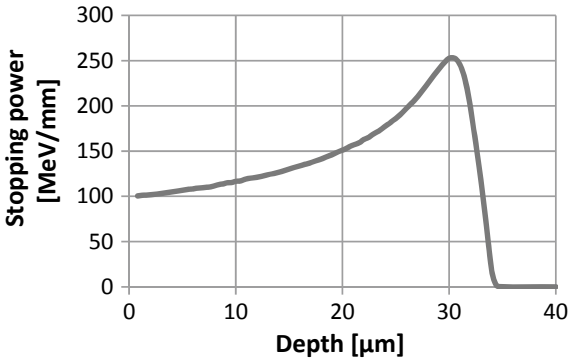

Fig. 3.7 The energy-loss curve of 5 MeV α-particles penetrating an elemental mixture representative for human skin (mostly H, C, O with $\rho_S = 1$ g/cm^3), a case discussed in 2.7. The particles feature an average range of 33.5 µm with a Bragg-Peak (maximum energy-loss) at 30 µm depth. At the right end of the peak the ions fully stop (= implantation)

$$x = \frac{1}{\rho_S} \int_0^{E_0} \frac{1}{S(E)} \mathrm{d}E \Rightarrow \mathrm{d}x = \frac{\mathrm{d}E}{\rho_S * S(E)}, \tag{3.9}$$

The underlying effects of stopping involve the collision between the projectile and single particles, leading to a statistical fluctuation of individual energy loss events. Figure 3.2 showed such an example and its result on the range. This statistical broadening of range and energy-loss is called straggling. Straggling broadens the particle distribution in energy and space, resulting in a beam energy distribution broadening at a fixed depth and a range broadening, respectively. The collisional nature of stopping induces not only a longitudinal variation of energy and range, but also a transversal component broadening the beam diameter. These statistical effects mostly follow a normal distribution (Fig. 2.22). The particles above and below the maximum see different $S(E)$. Due to the variations of S with energy the energy distribution becomes skewed. Figure 3.8 depicts the impact of straggling in an exemplary case at different depth. Practically effects of roughness and thickness tolerances over the finite beam spot sizes add up to the physical straggling. Due to their mass equalling the collision partner's mass electrons experience orders of magnitude intenser straggling than ions.

In contrast to electrons, ions can change their effective charge during passage of matter by picking up or stripping-off electrons. Equation (3.6) highlights the importance of the charge z for S. The change of charge state of ions mostly leads to fewer electrons attached to the nucleus for energies above some hundred keV. Because of this it is often called stripping (of electrons). The effective charge increases with increasing beam energy. Atoms with many electrons require energies even exceeding our 250 MeV limit for stripping off all electrons. The effect makes the initial projectile charge state practically irrelevant for stopping power. No matter whether a He atom, He^+, or He^{++} projectile, the stopping power remains the same, only the projectile

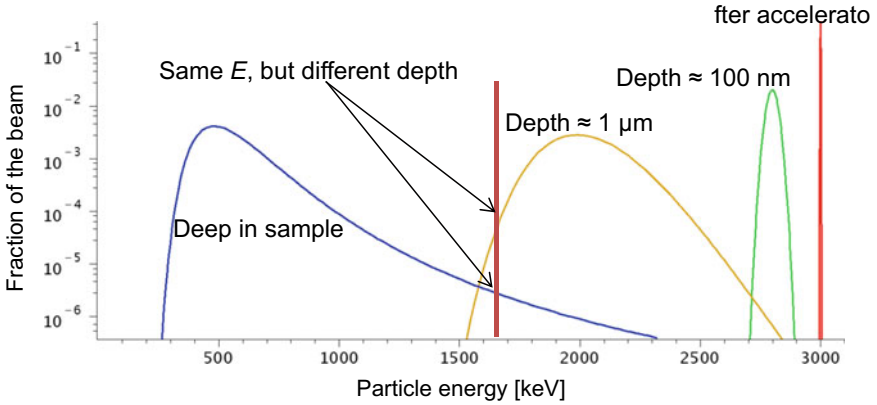

Fig. 3.8 Sketch of the beam energy distributions of 3 MeV ^{3}He ions in carbon at three different depth x. The deeper the particles reach, the broader and more skewed their energy distribution. As a result particles of the same energy can be found in different depth (vertical bar)

energy matters. The statistical nature of collisions also affects the effective charge, resulting in an energy-dependent statistical distribution of the charge states of the individual ions constituting a beam. Besides its impact on stopping power, stripping has a high practical relevance for ion beam generation and control. Examples such as the Tandem accelerator Sect. 2.2.1 and the negative ion extraction in cyclotrons Sect. 2.2.2 rely on stripping.

The effects discussed so far assume an evenly distributed electron cloud inducing the stopping. Gases and liquids fulfil this condition, but solids with crystallographic structure feature different, inhomogeneous electron distributions. Figure 3.9 illustrates such a distribution with several hotspots of electron density n_e and large areas of nearly zero electron occupation probability. The picture strongly depends on the crystallographic axis. Crystals appear as a stack of channels to the projectiles. When hitting a channel, the stopping significantly reduces due to the lower n_e, if the solid is sufficiently ordered and the particles hit in the crystallographic direction (practically that means normal incidence). In polycrystalline materials, the random grain orientation hardly leads to fundamental directions (the crystallographic indices with only ones and zeros) aligned to the surface normal, suppressing the effect. Only single crystals feature channelling. Channel acceptance angles increase with nuclear charges Z_1 and Z_2 of projectile and target, and decrease with projectile energy, since a pure coulombic interaction potential between the positive projectile and target nuclei charges forms the basis of this effect (Nastasi et al. 2014). In practice channelling yields information in crystallographic analysis of silicon wafers by MeV helium ions, achieving maximum acceptance angles in the order of 1° or by analysing the backscattering of focused electron beams from the individual grains in polycrystalline samples, see Sect. 7.1. The contrast derives from the fact that a backscattering into the acceptance angle (see Rutherford cross-section (3.1) has low probability, hence the projectile faces much lower stopping power than the backscattered products detected outside the acceptance angle.

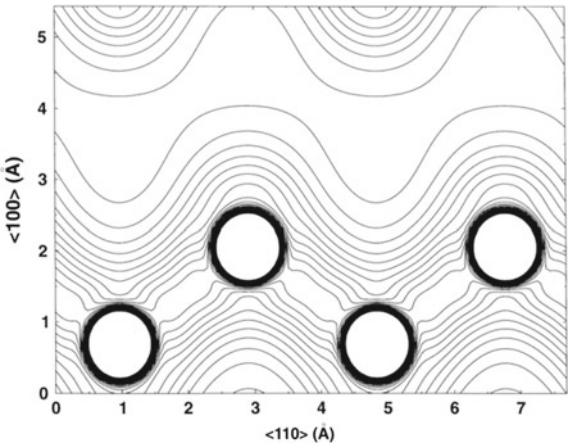

Fig. 3.9 The electron distribution of silicon in a < 110> †plane. The silicon atoms are clearly visible, as is the bond between the nearest neighbours. The contour interval is 0.05 e with contours going from 0.05 to 1.5. The electron density is high near the nuclei and low in between. Reprinted with permission from Elsevier from Sillanpää (2000)

3.3 Nuclear Reactions

– *Stupidity identifies itself by repeating the same action and expecting different results in each instance.*

This sentence, as true it is for real life, completely fails for the sub-atomic level of physics. The basic principle of quantum mechanics is uncertainty. Therefore it is indeed logical to expect different outcomes for every single beam particle impacting onto the same target. This fact should not be over interpreted, though. Summing up the outcomes over numerous interactions will lead to statistically solid probabilities, but it's just probabilities so everything remains possible.

Nuclear reaction cross-sections, or just cross-sections, describe the probability for a certain interaction pathway to happen. Graphically we can imagine them as a target disc which we try to hit with a projectile. In accelerator applications, usually the projectile, as a part of the charged particle beam, moves towards numerous targets atoms which are at rest. Every projectile sees the target discs of the many atoms it approaches, but still most of the space is empty making it improbable to hit a target. As a rule of thumb usually only up to a few percent of the projectiles undergo nuclear reactions. As with stopping nuclear reactions probe matter, independent of its arrangement in the form of density or porosity only the amount of passed atoms/area counts. In fact, generally many different nuclear reactions can take place between given projectile and target, each with its individual cross-section.

In order to describe the cross-section of a specific interaction, the unit barn ($= 10^{-28}$ m^2) was defined. We could think of it as the area of the imaginary target disc of each target particle. Its dimension is extremely small, but of course our projectile

will face many targets on its way, since the atomic density of matter is large. The probability P of interaction is given by the cross-section σ times the number of target particles N_T per target area A.

$$P = \sigma * \frac{N_T}{A} \tag{3.10}$$

Equation (3.10) applies independently to every constituent (element and isotope) of the target with their individual cross-section. Different types of reactions can occur with the same type of target. We already came to know the elastic nucleus scattering as relevant contribution to stopping at low energies or the elastic scattering with the electrons as primary contribution to stopping at higher energies. In contrast to elastic scattering, which conserves the total kinetic energy E, nuclear reactions are inelastic. Inelastic reactions enable a transfer between mass and energy, generally not conserving the kinetic energy (but of course the total energy). Due to the equivalence of mass and energy [Einsteins famous (2.6)], the physical law of conservation of energy remains intact. The Q-value expresses this energy redistribution in the quantity of energy transferred in the nuclear reaction (usually in keV). Consequently, elastic scattering reactions feature $Q = 0$ while inelastic reactions identify by $Q > 0$ (mass consumption) or $Q < 0$ (mass generation) defined by (3.11) for a 2-body reaction as depicted in Fig. 3.1.

$$Q = \Delta E = (m_1 + m_2 - m_3 - m_4)c^2 \tag{3.11}$$

Physically, the Q-value results from a difference in the sum of the rest masses, related to different nuclear binding strength, between the particles before and after the nuclear reaction. This so-called mass defect calculates from the difference in the actual nuclear mass from the sum of the masses of an equivalent amount of isolated protons and neutrons. The highest Q-values are found in reactions of light elements with ^{6}Li(^{2}H,^{4}He)^{4}He marking the summit with $Q = 22.38$ MeV. Very thorough studies with sub-keV precise nuclear mass data exist, summarised in the ongoing Atomic Mass Evaluation project(Huang et al. 2017) and made publicly available on numerous websites (e.g. http://oecd-nea.org/dbdata/data/structure.htm or http://nrv.jinr.ru/nrv/webnrv/qcalc). A few examples were compiled in Table 3.1.

The particles produced in a nuclear reaction can enter excited nuclear states, similar to excited atomic states, further reducing Q below the ground state mass difference. The nucleus features a shell structure of protons and neutrons similar to the atomic shell and its excitations as shown for three configurations of nucleon number $A = 14$ (^{14}C,^{14}N,^{14}O) in Fig. 3.10 (left). With enough energy provided by $Q + E$, nuclear reactions can produce ^{14}N in its excited state as the measurements shown on the right demonstrates. Here three different proton energies corresponding to three different Q-values of the ^{12}C(^{3}He,p)^{14}N reaction are detected. Most excited states quickly decay by emission of a photon with the corresponding energy, but even if the de-excitation is energetically possible, it can be hindered by the conservation of angular momentum. Every nuclear level features not only an energy, but also an angular

Table 3.1 Examples of mass defects (= binding energy), first 3 excited states, and coulomb barriers with protons. Protons naturally do not have excited states due to their single nucleon nature

Nucleus	P	4He	12 C	18O	18F	180Ta	181Ta
Mass defect (keV)	0	28,296	92,162	139,808	137,370	1,444,662	1,452,239
Mass defect (keV/nucleon)	0	7074	7680	7767	7632	8026	8023
Nuclear states (keV); (spin) (Parity)	0; 1/2+	0; 0+ 20,210; 0+ 21,010; 0−	0; 0+ 4438.9; 2+ 7654.2; 0+	0;0+ 1982.07; 2+ 3554.84; 4+	0; 1+ 937.2; 3+ 1041.5; 0+	0; 1+ 39.54;2+ **77.2; 9−**	0; 7/2+ 6.237; 9/2− 136.26; 9/2+
Proton Proximity barrier (keV)	181	364	1027	1338	1523	9555	9545

State transitions require spin differences of 1, otherwise the transition is forbidden and long-lived such as the 3rd state of ^{180}Ta also known as ^{180m}Ta. Proximity barriers from (Blocki et al. 1977). Nuclear levels from NuDat 2.7 [https://www.nndc.bnl.gov/nudat2] and Nubase2016 (Audi et al. 2017)

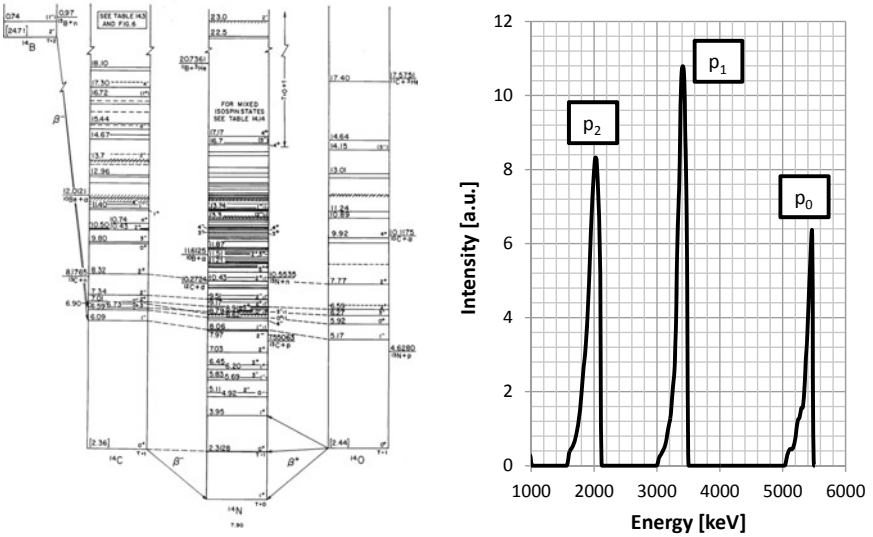

Fig. 3.10 Left: Nuclear levels of the nuclei with 14 protons + neutrons ($A = 14$). ^{14}N represents the only stable nucleus. All nuclei feature numerous excited states. From every state different pathways towards the lowest energy state exist via emission of particles and photons. In the ground state ^{14}O decays via β^+, while the first few excited states prefer emitting a proton forming ^{13}N. From(TUNL Nuclear Data Evaluation Project). Right: ^{12}C(^{3}He,p)^{14}N reaction at $E = 2.5$ MeV and 160° producing ^{14}N in the ground and the first two excited states. The emitted proton energy reduces corresponding to the excitation energy leading to three distinct proton peaks

momentum and parity. Physicists call transitions which have a difference of more than 1 unit of spin between initial and final level forbidden, since 1 corresponds to the spin carried (away) by a photon. Nuclear physics apparently makes it increasingly improbable to carry away more spin. The longest lived example for a forbidden excited state transition is ^{180m}Ta with a difference of 9–1 spin units between excited and ground state (Table 3.1) resulting in 1.8 * 10^{15} years half-life, but also other isotopes such as ^{99m}Tc feature practically relevant half-lives due to this effect.

Having fixed target situations in accelerator applications also requires a heavy moving particle after the reaction in order to conserve momentum. This prohibits a simple consumption of projectiles with only one product particle, but requires at least two products (2 variables need 2 equations). But nuclear physics further limits the possibilities. Nuclear reactions have to follow additional nuclear conservation rules, most importantly the conservation of particle number and electric charge. The amount of protons, neutrons, and leptons (namely electrons + neutrinos, see Sect. 4.4) will not change during the reaction, only a transfer between projectile and target is possible. The situation changes for β decays since these involve the weak force. In the β decay the conservation of lepton number becomes important. The conversion of a proton to a neutron, or vice versa, changes the nuclear charge which has to be compensated by emitting a positron or an electron, respectively. This violates the conservation of lepton count, consequently a neutrino or anti-neutrino, respectively, has to be emitted additionally. Physicists invented the so-called Feynman diagram to cover all possible reaction and decay routes, but this theoretical construct goes too far for applications. The actual probability and branching between different possible reactions is described by the individual reaction cross-sections or decay probabilities.

Not every reaction allowed by the conservation laws will also occur. Reactions with $Q < 0$ have a threshold since this missing energy has to be provided by kinetic energy of the projectile (conservation of energy). A chemist would call these endothermic and reactions with $Q > 0$ exothermic, but of course thermal energies have no meaning for the MeV energies involved in nuclear reactions. Since this book discusses charged particle beams and target nuclei also consist of similar charged particles, the electro-magnetic Lorentz force produces a barrier potential for reaching a nuclear proximity required for nuclear reactions. We can understand the nucleus as an armoured tank with its electrical charge building some kind of Coulomb armour. With projectiles of low kinetic energy fired for example from a handgun or a rifle we cannot penetrate its armour, but the projectile will bounce off. The more punch we have the higher the probability to penetrate the armour instead of bouncing off. The same applies to nuclear interactions, the higher the projectile energy, the lower the cross-section for elastic scattering and the higher the nuclear reaction cross-section. Table 3.1 lists a few examples of barrier potentials towards proton projectiles derived from analytical calculations. These barriers scale-up roughly with the number of protons involved in the reaction. The barrier energies only indicate at which projectile energies nuclear reactions become possible, but any barrier can be tunnelled in quantum systems. For this reason nuclear reaction cross-sections usually start with an exponential increase from low energies towards higher energies as the next section will elaborate.

3.3.1 Cross-Sections

In applications, nuclear reactions primarily involve ion beams. Nuclear reactions with electron projectiles require similar energies as with ions in the 10 MeV region, implying certain application drawbacks connected with the high electron velocity as discussed in Chap. 2. Furthermore, electron-nucleus reactions are somewhat limited by the fact that, in contrast to the constituents of ions, electrons are not present in the nucleus, limiting the possible reactions and products. For these reasons nuclear reactions with electrons have little application relevance and will not be discussed in this edition. Anyways, many physical aspects are independent of the projectile species.

The magnitude of the cross-sections strongly depends on the projectile energy and the projectile-target combination. In some cases also the nuclear polarisation state significantly influences the reaction cross-section (Ciullo et al. 2016). Nuclear reactions require higher energies than the elastic reactions underlying stopping due to the proximity of projectile and target required by the short-ranged nuclear forces responsible for nuclear reactions (Coulomb barrier effect). The evolution of the cross-section σ with the projectile energy E is described by the total cross-section $\sigma(E)$ (sometimes also just called cross-section). The example in Fig. 3.11 demonstrates the variation of the total cross-section of the $^{18}O(p,n)^{18}F$ reaction over five orders of magnitude between 2 and 200 MeV projectile energy. The cross-section first increases, then reaches a maximum of about 300 mbarn at $\approx$ 6 MeV, and then decreases towards higher energies again by five orders of magnitude towards 200 MeV. Empirically, many cross-sections follow a qualitatively similar behaviour with varying peak cross-section, peak width, and projectile energy at the maximum.

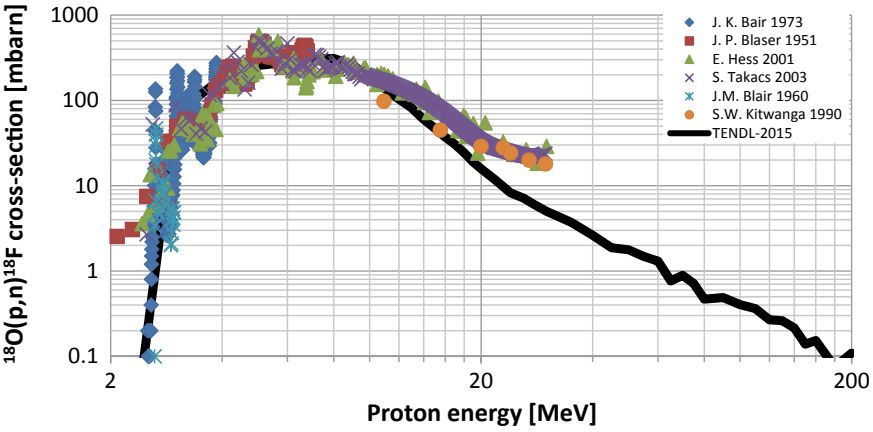

Fig. 3.11 An extract from the JANIS OECD Nuclear Energy Agency (NEA) (2017) database comparing experimental and theoretical differential cross-section for the $^{18}O(p,n)^{18}F$ reaction. Symbols mark experimental data, while the line shows calculated cross-sections from TENDL-2015 (Koning et al. 2015)

Figure 3.11 compares the semi-empirical cross-section TENDL-2015 (Koning et al. 2015) with various experimental data. All datasets roughly agree within a factor three to each other, but TENDL-2015 is unable to reproduce some of the features, for example the resonances in the 2–4 MeV region, which are, on the other hand, also ambiguous in the experimental data. The cross-section shows a typical threshold reaction, in this case $Q = -2438$ keV as displayed in the mass defect difference between ^{18}O and ^{18}F in Table 3.1. From the threshold on, the cross-section increases exponentially due to tunnelling of the proximity potential. For $Q \geq 0$ reactions, the threshold with its exponential increase will adapt to the order of the barrier potential. For ^{18}O(p,n)^{18}F the Coulomb barrier of 1338 keV is lower than the energy threshold (see Table 3.1) and therefore not relevant. The existence of resonances arises from the quantum mechanical particle-wave duality. Each particle has its individual wave and as soon as projectile and target wave come into contact, resonant overlaps, similar to the interference of light waves, can occur. The resonances change the cross-section at specific energies by orders of magnitude, either increasing or decreasing it. Towards higher energies, generally the cross-section decrease due to reducing particle wave-function overlap.

A moving projectile defines a unique direction/vector with its direction of movement. This vector represents a symmetry axis for the reaction, leading to a non-isotropic emission of reaction products. In other words, the cross-section changes with the angle towards the direction of movement, leading to differential cross-sections $d\sigma/d\Omega$ depending on the exit angle of the products, also called reaction angle, and projectile energy. Figure 3.12 shows an example. The quantity Ω describes the solid angle into which the given cross-section can be measured at the given energy E and reaction angle. Equation (3.12) allows calculating the solid angle from a given area A of a sphere of radius r. We can see it as a detector of area A with a distance of r to the point of reaction.

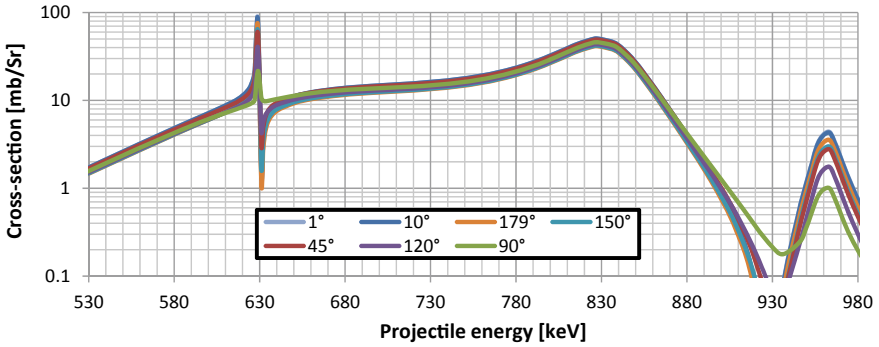

Fig. 3.12 Differential cross-section of the ^{18}O(p, ^{4}He)^{15}N reaction for detecting the ^{4}He at the stated laboratory reaction angles. The resonance at 629 keV is weakest at 90° and increases up to a factor 4 towards higher and lower angles. At 828 keV the cross-section decreases with increasing angle by about 20%. Data from Sigmacalc (Gurbich 2016) *R*-Matrix fits to experimental values

$$\Omega = A/r^2 \tag{3.12}$$

Differential cross-sections have a considerably lower level of available data in the literature due to the fact that determining them requires measuring the moving products in-situ and not only the amount of present isotopes at some point in time after the process (ex situ). Total cross-sections rather find use in isotope production and activation applications, while differential cross-sections find use in analytical methods due to their connection to detection and reaction kinematics. As in Fig. 3.11, the differential cross-section in Fig. 3.12 features an exponential growth from the low energy side and several resonances. In the differential form, a clear dependence of the resonance height on the reaction angle becomes visible. In $\sigma(E)$ only the angular average would be visible, but each resonance varies differently with reaction angle.

The determination of precise reaction cross-sections represents an integral part of many technological advances in accelerator applications, but also a challenging one. Physicists try to reduce the effort by determining only the data specifically required, leaving many holes in the data landscape. In many application cases discussed later in this book a certain element with several stable isotopes is used to produce a specific isotope via nuclear reactions. In this case, potentially several reaction types, usually sets of multi-product reactions such as (p,xn) can lead from different isotopes to the same nuclide. In this case the individual isotopes reaction cross-sections were summed up to a so-called production cross-section. Production cross-sections are a simplification with several drawbacks, but the advantage of easy experimental determination using natural isotopic composition. As an example ^{182}Re via protons could occur from natural tungsten from reactions with its various isotopes via ^{182}W(p,n)^{182}Re, ^{183}W(p,2n)^{182}Re, ^{184}W(p,3n)^{182}Re, or ^{186}W(p,5n)^{182}Re reactions. If we measure only the final ^{182}Re activity we will not be able to distinguish between the isotope specific reactions. In contrast, the reaction cross-sections could be determined only with an isotopically purified target of a single (tungsten) isotope.

Unfortunately, theoretical physics has not proceeded to a point where mathematical descriptions for all nuclear scattering reactions exist. We already saw the Rutherford cross-section in (3.1) with its accurate theoretical description of elastic scatterning up to a few MeV as an example of such a theoretical description, but the underlying reaction does not involve a nuclear interaction in the sense of everything beyond the electrical charge visible to the outside (the billiard ball model). Existing approaches based on quantum calculations on the quark level (Quantum-chromodynamics) offer the potential for delivering theoretically derived cross-sections, but the computational effort strongly scales with the number of involved quarks and brings current supercomputers to their limits, even for hydrogen isotope reactions. A full solution of the problems probably requires the next level of computer technologies, more complete physical understanding of the strong nuclear force or of the four fundamental forces in general.

Nuclear physicists found a set of models describing nuclear reaction cross-sections to inter- and extrapolate from given experimental data. These semi-empirical equations combine an adequate theoretical model description of the overall process and

require fitting of (theoretically) unknown parameters to the experimental data. This procedure yields a formula for calculating cross-sections over a certain energy and angular range with a statistical uncertainty given by the data. The problem is, the range of validity is not known and systematic errors in the experimental data or model could be unwillingly absorbed in the result. Hence semi-empirical models are a useful tool for data analysis and computations, but the results must be handled with care, especially in the extrapolation region where the risk of systematic errors of the model increases.

$$\sigma_{\mathrm{Res}}(E) \sim \frac{1}{(E - E_{\mathrm{Res}})^2 + \Gamma^2/4} \tag{3.13}$$

In general, reaction cross-sections combine resonant and non-resonant regions. We already learned the start of nuclear reactions follows an exponential increase due to the tunnelling of the Coulomb barrier. The Breit-Wigner or also Lorentz resonance function (3.13) describes the probability distribution of resonant interactions. This cross-section depends on the central energy of the resonance E_{Res} and a resonance width Γ. Interferences with the non-resonant part of the reaction can lead to the typical down-up or up-down resonance where both cross-sections subtract and add up (or vice versa) before and after the resonance energy. Figure 3.13 shows three examples of this process with different Γ in all cases.

The next level beyond this simple analytical fitting requires more complex models implemented in several codes. Implementing the above idea of resonances and the interaction of particle waves in the sense of the Schrödinger equation leads to the so-called R-Matrix algorithms such as the code SigmaCalc (Gurbich 2016). These fitting algorithms combine the features of several states (3.13) known from experimental data to a matrix which then allows solving the Schrödinger equation, reproducing cross-sections in the resonant and non-resonant region over an energy and angle

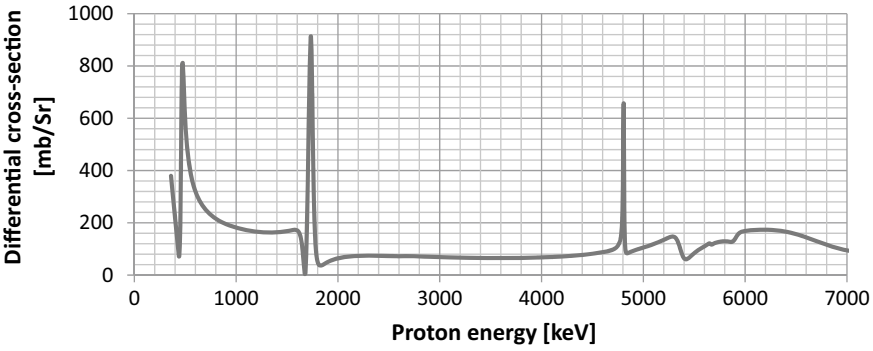

Fig. 3.13 Differential cross-section of $^{12}C(p,p_0)^{12}C$ at 165°. Already at 360 keV this elastic reaction deviates from the Rutherford behaviour, in spite of the 1027 keV barrier. The data show several types of different resonances in the given energy range. Data from *R*-Matrix fit of SigmaCalc (Gurbich, 2016) to a set of experimental data

range given by the experimental data. Nuclear models such as the codes Talys (this is behind the frequently updated TENDL cross-section database) or Empire (Herman et al. 2007) follow a different approach by combining a multitude of limited physical models of specific nuclear interactions. These codes produce reasonable total cross-sections as we saw in Fig. 3.11, although resonant features might be missing. For differential cross-sections the agreement significantly worsens. Nevertheless, these codes often provide the only available data for new developments and over the years progress on the underlying nuclear data continuously improves the result quality of these codes.

Knowing what cross-sections are, the applicant will ask how to determine them experimentally. Cross-sections represent a probability at a given energy. Consequently, we required a defined known energy for the reaction in the target, an identification of the reaction, and a detector for counting the amount of reaction products in relation to the fluence of projectiles. For detecting the occurrence of a given nuclear reaction we have to detect the products of this reaction. This could be the fast light products (mostly p, α, and n) or the heavy product, which usually remains in the target due to its limited range. Stopping reduces the initial beam energy, leading to a mixing of different energies upon passing a target. This requires either a local measurement, an energy resolved measurement, or a restriction of stopping by using thin targets and large detector solid angles for compensation.

Differential cross-sections are mostly measured via thin targets. The exact quantity depends on the element and beam energy, but typically lies in the order of 1 μm thickness. The target thickness induces a contradiction due to the well-defined energy with thinner samples (lower stopping), but the higher statistics with thicker samples (3.2). The detection of the heavy products follows the beam irradiation via ex situ spectroscopy of the decay radiation together with isotope identification via characteristic spectral libraries available for most isotopes, e.g. (Nucleonica GmbH 2014). This pathway yields differential cross-sections. For non-monoisotopic target elements, similar reactions potentially lead to the same product isotope. (p,xn) reactions are the prime example, but also other reactions, decays, or impurities lead to the same problem. In this situation only isotopically enriched targets allow unfolding the problem with an ex situ analysis.

In-situ detecting the light product via particle detectors suffers from the problem of catching all angles around the target via physical placement of detectors. A differential cross-section results from a single detector angle. The in-situ detection allows for an energy resolved measurement of the products. This additional information in principle allows unfolding the stopping for 2-body reactions and using thick samples to generate complete spectra in one measurement. The backward calculation of the kinematics (see next section) has its drawbacks, but offers the potential for accelerated determination of cross-sections via stopping induced beam energy scanning (Möller S., Analytical continuous slowing down model for nuclear reaction cross-section measurements by exploitation of stopping for projectile energy scanning and results for 13C(3He,α)12C and 13C(3He,p)15N, 2017). In the end the best method derives from the energy range, the required accuracy, and the specific reaction to be investigated.

3.3.2 Kinematics

The cross-section describes which reactions occur with which frequency/probability when a given beam impinges on a target. Kinematics describes how the particles move into, and, in particular, out of this reaction. The most important choice for understanding kinematics relates to the inertial system considered. In other words, what do we see as resting and what as moving? As always in this book, we have a moving beam particle and a stationary target defining our initial conditions. This is called the laboratory (Lab) system, the interial system we also reside in. Nuclear decays feature only a single stationary particle in the beginning, significantly simplifying the situation as no preferential direction or relative velocity exists. Due to this symmetry, decays simply emit their products isotropically (equally probable in all directions) and will not be considered primarily in this section.

The Centre-of-Mass (CM) system represents the true physics of each interaction. In this system both projectile and target move, but with exact opposite momentum. In collider experiments, two beams move towards each other, making the CM system identical to the Lab system. All other cases require re-calculation of energies, angles, and cross-sections to switch between both. The Lab system represents our, and in the case of stationary targets, the targets point of view. For applications we are interested in the Lab system, since it describes the results we see. Switching from Lab to CM system reduces the kinetic energy available for reactions. In the Lab system, the centre of mass, as a point in between projectile and target, has to move towards the target. A kinetic energy and momentum not present in the CM system. This CM movement could be understood as a virtual particle carrying the remaining kinetic energy. The recalculation between CM and Lab and the view of the CM system belong to the fundamental particle physics or nuclear physics and will therefore be omitted in this book. For more details on the calculations related to this, the reader is referred to any standard nuclear physics book.

The physics of nuclear reactions and decay kinematics depends on the number of involved particles. Each particle existing before and after the reaction has a set of kinematic properties, namely mass (m), kinetic energy (E), and movement vector (v) or in other notation energy and momentum vector. In applications only very few reactions involve more than two particles on the input side, due to the small probability of coincidence for the usual beam densities. This means we consider reactions of a projectile with a target. Already in Sect. 3.3.1 we learned about the existence of reactions with two products such as ^{181}Ta(p, n)^{181}W with a light product, the neutron, and a heavy product. The wording of light and a heavy product originates from nuclear reactions favouring to form the strongest bound products (see Fig. 8.1), which are typically heavy elements. Correspondingly nuclear reactions tend to release neutrons or protons or if the Q-values are attractive ^{4}He. These so-called 2-body reactions yield a unique solution for the kinematics of the products. Figure 3.1 depicts the 2-body situation. The application aspect of the kinematic theory starts when not all kinematic properties are known. Solving 2-body kinematics relies on the mathematical logic of requiring as many equations as we have unknowns, see (Zagrebaev et al. 2019) for an

online tool. The conservation of energy and momentum vector, see (3.14), provides the equations. Particle 1 (bearing E_1, p_1) represents the projectile, particle 2 the target and particles 3 and 4 the products. Particle 3 represents the light product and particle 4 the heavy product particle. Consequently, if we know all kinematic properties of an interaction except for two (remember each particle bears two properties), the kinematic equations will yield unique results for the two unknowns.

$$\begin{aligned} \overrightarrow{p_1} + \overrightarrow{p_2} &= \overrightarrow{p_3} + \overrightarrow{p_4} \\ E_1 + E_2 &= E_3 + E_4 \end{aligned} \tag{3.14}$$

Here the momenta are given as vectors. The pure forward momentum of the initial situation can receive an additional transversal momentum component balanced between the two product particles. Since two particles necessarily lie on the same plane, the whole situation becomes rotationally symmetric about the axis defined by the movement vector of the projectile towards the target. This rotational symmetry is the same as discussed with the reaction angle in Sect. 3.3.1. With the target (particle 2) initially at rest, p_2 and E_2 become zero. Reactions with $Q \neq 0$ break the conservation of mass by opening an exchange channel between mass and kinetic energy. We need to take the transfer between mass and energy via the Q-value into account. This modifies the conservation laws of (3.14) to

$$\begin{aligned} p_1 &= p_3 * \cos(\theta) + p_4 * \cos(\phi) \\ 0 &= p_3 * \sin(\theta) - p_4 * \sin(\phi) \\ E_1 &= E_3 + E_4 - Q \\ m_1 + m_2 &= m_3 + m_4 + Q/c^2 \end{aligned} \tag{3.15}$$

In production applications we usually know the projectile and target properties, while in analytical applications projectile and the properties of one or two products are known from detectors. The solution for a missing quantity, such as a product energy, is anything but straightforward. According to (Nastasi et al. 2014) Appendix 4, the product energies in the Lab system read in the non-relativistic case with $E_2 = 0$:

$$E_3 = \frac{E_1 m_1 m_3}{(m_1 + m_2)(m_3 + m_4)} \left[\cos(\theta) \pm \sqrt{\frac{m_2 m_4}{m_1 m_3}\left(1 + \frac{Q}{E_1} + \frac{m_1 Q}{m_2 E_1}\right) - \sin^2(\theta)} \right]^2 \tag{3.16}$$

$$E_4 = \frac{E_1 m_1 m_4}{(m_1 + m_2)(m_3 + m_4)} \left[\cos(\phi) \pm \sqrt{\frac{m_2 m_3}{m_1 m_4}\left(1 + \frac{Q}{E_1} + \frac{m_1 Q}{m_2 E_1}\right) - \sin^2(\phi)} \right]^2 \tag{3.17}$$

$$\theta_{\max} = \arcsin\left(\frac{m_2 m_4 (E_1 + Q)}{m_1 m_3 E_1}\left(1 + \frac{m_1 Q}{m_2 (E_1 + Q)}\right)\right)^{0.5} \tag{3.18}$$

$$\sin(\phi) = \left(\frac{m_3 E_3}{m_4 E_4}\right)^{\frac{1}{2}} \sin(\theta) \tag{3.19}$$

The book (Nastasi et al. 2014) provides a comprehensive list of kinematic equations beyond (3.16)–(3.19) in its appendix. The equations include the possibility of elastic ($Q = 0$) and inelastic ($Q \neq 0$) nuclear reactions by allowing for different masses of incoming (m_1, m_2) and outgoing particles/products (m_3, m_4) and a kinetic energy production or consumption via the Q-value. Equations (3.16) and (3.17) offer two possible solutions ($\pm$) depending on the mass ratio of projectile and target. For a projectile lighter than the target, both products could be scattered in the forward direction (think of a grazing impact) or in opposite directions (think of a frontal impact). If the projectile mass equals the target mass or exceeds it, both products have to move in the forward direction due to conservation of CM momentum. Only one solution remains.

In other words, for a given set of properties of one product, the properties of the second product are strictly defined by the conservation laws. Practically this means, if we analyse one product for its energy and mass at a certain scattering angle, e.g. Θ, and we know the projectile mass, the 2-body kinematics, e.g. in the form of (3.16), can tell us for example which mass the target had. In this case m_2 and m_4 are two unknowns, but we can add the conservation of mass from (3.15) as the second equation required for a unique solution with 2 unknowns. In some cases logical exclusion principles yield extra information on the involved particles via conservation of nuclear numbers (proton, neutron, electron count) or known Q-values. This recalculation represents an important fact for accelerator based analytics by making the measurement of different quantities physically equivalent for understanding the whole reaction.

3-body or n-body reactions such as (p,2n) or (p,xn), respectively, follow different rules than 2-body reactions. The definition of the kinematic properties of one product does not define the kinematic properties of the other two products, since these two have no mathematical rule how to share the remaining energy and momentum. Energy, momentum, and mass are still conserved, but the additional degree of freedom yields distribution functions instead of singular values as depicted in Fig. 3.14. Imagine dropping a bag of food onto a bunch of dogs: All the food will be consumed for sure, but each time you do it every single dog will receive a different amount of food. This n-body situation is independent of whether a projectile-target situation or a decay such as the β^- decay emitting a heavy decay product, an electron, and an anti-neutrino is considered. A prominent example of this problem is the KATRIN experiment searching for the neutrino mass via detection of the energy distribution function of the electron emitted in the decay of tritium. The problem of this analytical experiment lies in the decreasing counting statistics towards the high-energy end of the electron energy distribution.

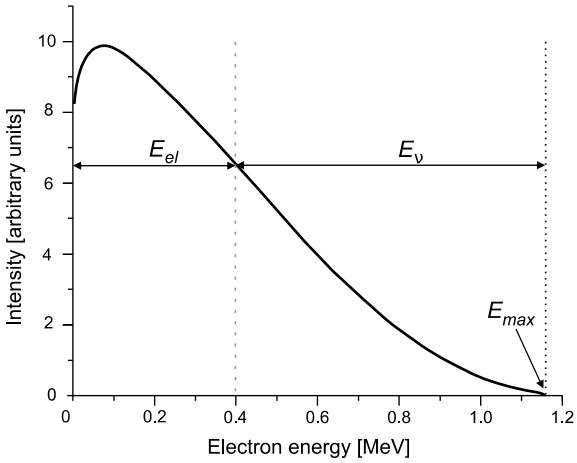

Fig. 3.14 Energy spectrum of the electrons escaping from the β-decay of ^{210}Bi, which is a 3-body decay (heavy nucleus, electron, muon). Due to their kinematic freedom n-body decays always feature product energy spectra. The example shows an electron energy $E_{\mathrm{el}} = 0.4$ MeV would correspond to a neutrino energy $E_{\mathrm{v}} = 763$ keV, but all other combinations are also possible

In the distribution function lower energies occur more often, since more allowed combinations of properties for the other particles exist in this region. Physicists call this the density of states. Considering the limiting case of one particle receiving the maximum possible energy (E_{Max}), the other two particles have to feature an exactly opposite momentum, due to the limited available energy, and only one state of the whole system remains possible. For simplifying the situation we can reformulate the problem to a 2-body reaction with an imaginary box combining two of the three products to one. In any case the physics of ambiguous solutions remains the same, making n-body reactions an at least unattractive situation for analytics.

3.4 Depth- and Stopping Dependent Reactions

Considering the individual particle picture, a charged particle traveling through matter constantly loses energy, but it also has a probability to scatter depending on energy and projectile-target combination. Combining these effects yields the reaction probability of a nuclear reaction described by the cross-section σ in a depth interval of z to z_1 or energy interval E_0 (= beam energy) to E_1, respectively. In the energy picture, the ratio of the reacting ρ_{R} to the stopping ρ_{S} matter comes into play when considering compounds consisting of several elements. In these mixtures, all target particles induce stopping, constituting ρ_{S}. Only specific target species interact via σ, constituting ρ_{R}.

$$W \equiv \int_{z_1}^{z} \frac{\Delta W(E)}{\Delta x} \mathrm{d}x = \int_{z_1}^{z} \sigma(E(x)) * \rho_{\mathrm{R}} \mathrm{d}x = \frac{\rho_{\mathrm{R}}}{\rho_{\mathrm{S}}} \int_{E_1}^{E_0} \frac{\sigma(E')}{S(E')} \mathrm{d}E' \tag{3.20}$$

Equation (3.20) describes the reaction probability W in 3 different forms. First the reaction in an infinitesimal slice of the target of thickness Δx integrated over the considered depth, second the energy (E) dependent cross-section times the reaction partner density integrated over depth and lastly the depth is solved for the depth dependent energy via the means of the stopping power S. Setting $E_1 = 0$ assumes full stopping of the projectile in the target, a situation typical for accelerator applications. For analytical purposes the reaction depth will be important to resolve further information such as depth and local concentrations of elements and isotopes ρ from the analysis. For production purposes, the integral over the whole accessible depth, the range, or the integral over the energy from the initial accelerator energy to zero, respectively, is more relevant. In either case, the relevant quantities change over depth and this location/depth of reactions happening forms a quantity of interest.

Figure 3.15 explains the different parts where stopping and depth define the reactions and whether products remain in the sample or leave it. Projectiles entering the target at a shallow angle, i.e. α close to 90°, induce reactions closer to the surface. The depth of the reaction scales according to (3.21). Variation of the impact angle enables virtually increasing the stopping power of the material for the projectile. The same scaling exists for the exit angle of the products, enabling differentially changing the effective stopping of projectile and products, a trick often used to increase for example the depth resolution of analytical methods. Unintended impact and exit angle variations relate to surface roughness and porosity.

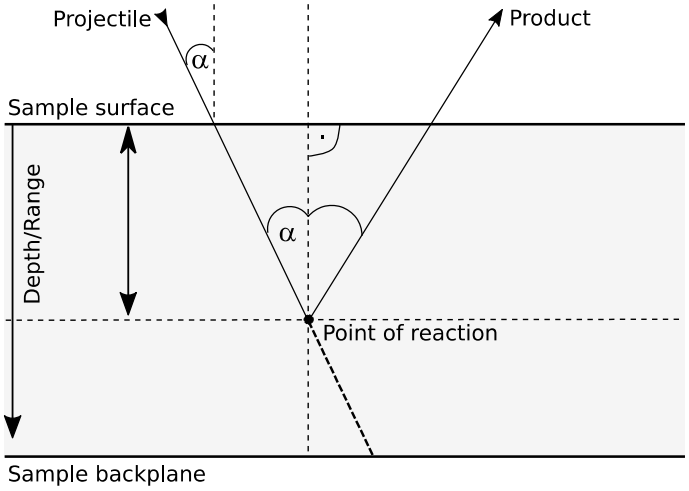

Fig. 3.15 An exemplary depth dependent scattering situation. The way in and out of the sample differ depending on impact and exit angles. Leaving the sample requires sufficient product energy, depending on depth and exit angle of the products

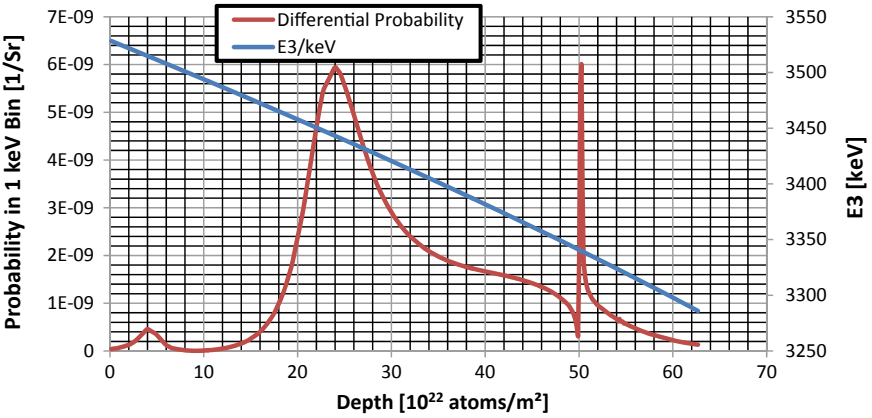

Fig. 3.16 Depth calculation of the ^{18}O(p, ^{4}He)^{15}N reaction of 988 keV protons in SiO_2 showing the depth profile of reaction probability together with the light product (^{4}He) energy E_3 at 150° scattering angle. The reaction has a range of about 6.2 * 10^{23} atoms/m^2 (recalculate with density to have it per length) with a lower energy limit of 520 keV due to the onset of the reaction barrier, see Fig. 3.12

$$\text{Depth} = \text{Range} * \cos(\alpha) \tag{3.21}$$

Considering a perpendicular incidence, $\alpha = 0$, of a proton probing for ^{18}O in a SiO_2 (silicon dioxide) and combining Fig. 3.15 with the (3.19), (3.20), and (3.16) yields Fig. 3.16. Here we calculated depth in the sample in units of atoms passed vs. the light product energy E_3 at 150° scattering angle for the reaction ^{18}O(p, ^{4}He)^{15}N (cross-section in Fig. 3.12) with 988 keV projectile energy E_1. For recalculation of this two-body reaction kinematics take care of the units and magnitudes. Note that the calculated E_3 is given at the depth of the reaction, when leaving the sample additional energy will be lost on the way out. Neither was straggling included.

The figure demonstrates several aspects of depth dependent reactions. The light product energy changes with depth, but in this case only by about 243 keV, while the projectile energy changes by 468 keV. The origin of this discrepancy lies in the reaction $Q = 3979.8$ keV, adding additional energy to the kinematics which dominates the momentum conservation in the two-body kinematics. In the reaction probability, the cross-section clearly becomes visible, as stated by (3.20). If this reaction was used for analytical purposes, the behaviour of the cross-section leads to a low sensitivity to ^{18}O close to the surface (<15 * 10^{22}atoms/m^2). The two resonances at 25 and 50 * 10^{22} atoms/m^2 on the other hand produce strong signals in limited depth ranges. At depth beyond 62 * 10^{22} atoms/m^2, the sensitive range but not the projectile range ends, since the cross-section exponentially approaches the reaction Coulomb-barrier.

Applying this setup for example to a heterostructure, which features a significant ^{18}O concentration only at the surface, e.g. due to a ^{18}O tracer gas exposure, only negligible amounts of detectable products will be produced. The method will not be sensitive to the sample structure. The method is right, but the projectile energy

was wrongly configured. Changing the projectile energy E_1 from 988 to the 830 keV (cross-section resonance) optimizes the detection properties via the understanding of depth dependent reactions.

In most applications, efficient usage of the expensive accelerator technology is a central aspect. The term *efficiency* always requires specification of the quantity the process makes optimal use of. In this case we are looking for energy efficiency, since it not only determines a part of the application cost structure, but it also defines target heat load and radiation safety aspects. Here in particular the stopping dependency of reactions influences the result. Applications usually require a defined amount of specific reactions, therefore the optimal beam energy and current have to be found before installing and setting up the accelerator. Considering the full (average) track of the projectiles via depth dependent calculations allows us understanding this efficiency. Instead of calculating the beam energy with maximum reaction probability W, we have to add the input projectile energy E to (3.20) to obtain a quantity representing production efficiency H:

$$H(E) = W/E \tag{3.22}$$

The maximum of (3.22) yields the point of maximum beam energy efficiency. In other words: For a required reaction rate, corresponding for example to a production rate of isotope X, the maximum in H represents the minimum in required input beam power. Technically spoken this energy marks the point where increasing the beam current yields the smarter choice than increasing the beam energy. The evolution of H depends on the fundamental physics of S and σ and their evolution. Mathematically, the maximum in H corresponds to a zero-point in its derivative. Of course several local maxima can be present, e.g. when the reaction cross-section σ features several maxima/resonances.

$$\frac{\mathrm{d}H(E)}{\mathrm{d}E} = 0 \tag{3.23}$$

Equation (3.23) tells us the shortest and most efficient route to our production goal by minimizing the costs for the accelerator (Beam energy E_0), electrical power input ($E_0 \times$ current I), and target heat loads (also $E_0 \times I$). Will every reaction have this zero-point? A zero-point in the slope of H corresponds to the reaction cross-section decreasing faster than the stopping power.

Let us consider a specific case. For inducing nuclear reactions typically some MeV of projectile energy are required. For light ions this value lies beyond the maximum in stopping power (typically between 0.1 and 1 MeV, see Fig. 3.6), hence the stopping power monotonically decreases for higher projectile energies for any target. The nuclear reaction cross-section on the other hand can be very dynamic with resonances or at least a single broad resonance at a few MeV. Figure 3.17 compares S and σ with the ^{18}O(p,n)^{18}F reaction used for producing ^{18}F-PET tracers (see Sect. 6.1). The reaction features a simple single resonance cross-section and a threshold around 2.5 MeV, qualitatively similar to many other reactions, check

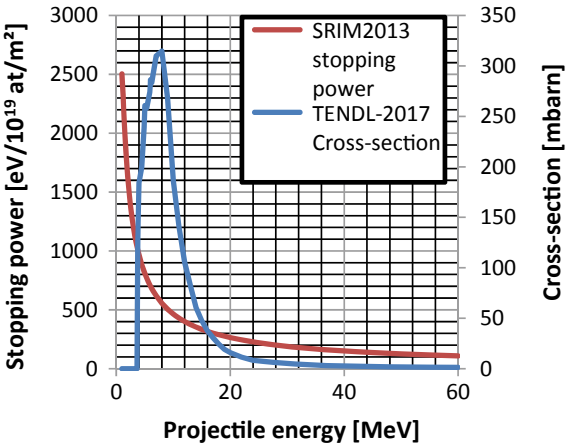

Fig. 3.17 Plot of the evolution of stopping power and nuclear reaction cross-section of ^{18}O(p,n)^{18}F used for the production of ^{18}F labelled medical products in ^{18}O enriched water ($H_2^{18}O$)

(OECD Nuclear Energy Agency (NEA) 2017). At low energies, S decreases while σ increases, but above the maximum in σ at 8 MeV both decrease.

Ok, if both values decrease we have to dig in deeper. The ion stopping power of (3.6) demonstrated a decrease of stopping power with something like $\ln(E)/E$, while the resonance of cross-section in the form of (3.13) decrease with $1/E^2$, a faster decay. The ratio σ/S then scales with $1/(\ln(E)E)$ resulting in a monotonic increase of the integral over this ratio. The integral of this function yields $\ln(\ln(E))$. Taking into account the proportionally to the beam energy increasing invested energy of (3.22) we end up with $\ln(\ln(E))/E$. These functional shapes we will also see in Fig. 3.18.

What can we do for increasing the output of a given reaction when beam energy is fixed? In numbers this efficiency means: At 12 MeV the reaction probability reaches 0.33% compared to, for example, 0.46% at 24 MeV. With 24 kW beam power (12 MeV/2 mA or 24 MeV/1 mA) we obtain 4.1 * 10^{16} reactions/s at 12 MeV, but only 2.8 * 10^{16} reactions/s at 24 MeV. The 46% higher efficiency at 12 MeV comes along with less unwanted activation, but also about 3 times increased power load on the target window required for the water target.

Figure 3.18 compares the energy efficiency of the ^{18}O(p,n)^{18}F reaction by production per projectile and per MeV invested energy. The figure shows a strong increase of efficiency starting at a few MeV, originating from the simultaneous decrease of the stopping power and increase of the reaction cross-section as displayed in Fig. 3.17. Between 20 and 30 MeV this increase levels off at a reaction probability in the typical order of 1%, here 0.5–0.6%. While the reaction probability still increases slowly, the efficiency factor H stagnates, its derivative approaches zero. At this point the accelerator layout would suggest rather increasing the accelerator current than its energy, since both deliver an identical benefit for the production rate. Increasing the beam

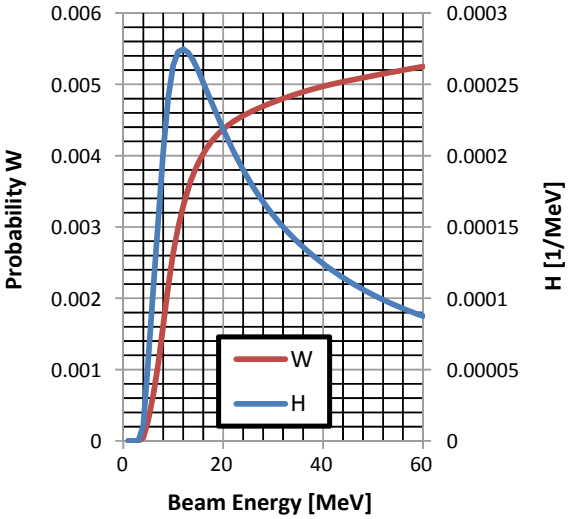

Fig. 3.18 The integration of (3.20) from the energy given on the *x*-axis down to zero represents the reaction probability for the $^{18}O(p,n)^{18}F$ on the whole path of the proton projectile till its stop in the H_2O target. Above the cross-section maximum at 8 MeV the slope of both curves strictly reduces with a maximum in H at 12 MeV

energy yield more problems of radiation protection and device cost, while increasing the beam current does not.

For electrons, the situation is upside-down and we see a minimum of the stopping power in the order of 1 MeV with increasing stopping power towards higher energies. When considering the energy efficiency of a reaction this induces a generally bad situation, since the minimal stopping power coincides with the lower limit for nuclear reactions. To be fair to the electrons: Electron stopping powers are lower than ion stopping-powers in the considered range, see Fig. 3.6.

Practical and economic aspects limit the maximum beam energy in applications. Physical limits require given minimum energies in order to induce the foreseen reactions as well as reach required penetration depth'. In this section, we learned how to navigate in the grayscale between these extremes via the physics of depth dependent reactions. As an example consider an electron microscope: At higher electron beam energy additional elements become visible by enabling more X-ray transitions (Fig. 3.4), but if the measurement aims at analysing a thin layer, e.g. a thin coating on a thick substrate, higher beam energy would finally lead to information mixing of layer and substrate, since increasing electron energy increases the projectile range, penetrating the thin layer.

3.5 Computer Modelling

Computer modelling of particle-matter interaction processes has become the main tool to derive quantities for accelerator applications, radiation protection purposes, and the layout of new devices. The complex equations presented in this chapter require a computer based treatment due to the large amount of considered reactions, individual properties, and experimental data input. In real world problems, the geometry and time-evolution add additional complexity to the housekeeping of the processes. In spite all these complications, modelling based on the best knowledge usually hits the reality within a factor 3 and often even better. Therefore computer models enable a full construction of basically all applications presented in this book in the idea of computer aided design (CAD).

Unfortunately, no single software combining all accelerator application aspects exists so far, but different programs need to be combined as modules for modelling an application setup. This starts with beam optics (see Sect. 2.3), thermo-mechanical modelling (e.g. Sect. 2.6), radiation protection (Sect. 2.7), and ends with beam matter interaction, namely stopping, nuclear reactions, detectors, and decays.

Let us first consider the peculiarities of a practical situation in a qualitative manner using an example featuring the main points of many applications. The considered example is a spallation neutron source with a proton beam of some hundred MeV and a tungsten target where the beam releases neutrons via (p,xn) reactions. These neutrons supply several experiments including a medical patient treatment. The beam produced in the accelerator part travels towards the neutron production target through stainless steel 316 vacuum tubes. The beam has a finite emittance; hence at least a minute fraction of the beam continuously hits the beam tube, considering a normal distribution. For the machine layout, we need to know if it will be possible to exchange steel parts for maintenance (radioactive inventory limits) and how far away vacuum pumps and electronics have to be placed in order to survive the radiation. At the target, the beam impacts the tungsten metal and suffers the continuous stopping. As we learned in the last section, relevant changes of beam energy and nuclear reaction probability occur already on the μm scale. Furthermore, tungsten consists of five natural isotopes (+impurities) each having around 20 different reactions above 100 MeV. For the treatment of patients this primary spectrum, originating from the proton reactions, is too broad. The primary neutrons interact with their surroundings, leading to thermalisation, reactions, and broadened neutron spectra. The produced neutrons on the other hand interact only weakly, with relevant changes on the 10 mm scale. A clever placement and material selection of structures and coolant flows significantly affects this spectral broadening and reduces the dose to the patient for a given treatment result. Finally, the neutrons interact with the patient. To allow the patient to survive the treatment only limited radiation doses/exposure times can be applied in order to avoid introducing more problems than we solve. This knowledge needs to be present before treating the first patient, but it strongly couples with the building and accelerator and target layout. Both can hardly be altered after installation. Simulations and also practical testing of components become necessary.

Following the nuclear interactions of potentially thousands of particle species (currently over 3000 isotopes are known) in 4D space-time is a mathematical and computational challenge. Two main mathematical approaches allow for a solution of these systems. In the first approach, large systems of analytical equations such as (3.24) enable an exact and computationally inexpensive solution on the time scale of minutes. The equation calculates the density N of all n involved isotopes/nuclides over the application time t via losses by exponential decays with half-lifes λ and the production from the decay of mother nuclides. Unfortunately, these advantages are countered by the difficulty to include complex geometries in the equations. Reasonable approximation of real situations by idealised physics allows an application of the analytical formalism to real situations. In our spallation example, the activation of the beam tube forms such an example. The produced quantities of activity are small, do not couple back to the beam or its surroundings and the distribution is homogeneous along the beam, since only very few beam particles get lost to the tube wall. The coupling of geometry to the nuclear interaction remains small, allowing neglecting it and assuming the beam tube as a point object receiving an input flux of ions. Even if additional interaction hot-spots such as apertures exist, these can be treated independently with an individual equation set.

$$N_n(t) = \sum_{i=1}^{n} \left[N_i(0) * \left(\prod_{j=i}^{n-1} \lambda_j \right) * \left(\sum_{j=i}^{n} \left(\frac{e^{-\lambda_j t}}{\prod_{p=i, p\neq j}^{n} (\lambda_p - \lambda_j)} \right) \right) \right] \tag{3.24}$$

In the second, so-called Monte-Carlo approach, codes simulate the hypothetical life of single particles through the given application geometry. This includes its movement, reactions and daughter particles. When interacting with matter, the particles have a certain probability of having one or another reaction and it is just decided by the throw of a virtual dice which of those marks the particles destiny. Naturally, less common situations become statistically underrepresented but yet may be important. Consequently, an accurate result requires a large amount of test particles to catch all possible situations, but the statistical question mark will always remain relevant. Furthermore, the time domain becomes difficult to access, since every point in time requires a simulation of the full geometry. In the spallation example, all site and construction related aspects are best solved using Monte-Carlo methods. Running several million test particles through the building will produce as many different particle histories, but most of the building volume will also get probed by these test particles. The simulation approximates the building and the beam conditions to be constant.

For calculating the inventory of daughter nuclides following a nuclear reaction process, the individual decay pathways of each nuclide have to be followed and the quantity of each daughter depends on the quantity of all its ancestors due to the connection by decay. The problem arises not only after a beam irradiation, but also during the beam irradiation since these daughters can also react with the beam forming new nuclides otherwise not accessible. This further complicates the full process to a complex coupled equation system. The Bateman-equation, (3.24),

describes the situation without source term (production by beam interaction) with the half-life time constant λ_n, the quantity N_n of a certain nuclide n. The decay chain starts with the mother nuclide $n = 0$ at time t and evolves for all the daughters i. Adding a source term and a physical library of nuclide data to this equation leads to the basis of a first application code such as FISPACT-II (Culham Centre for Fusion Energy 2018).

FISPACT-II implements the mathematical solution of (3.24). Equation (3.24) also demonstrates the strength of this approach, since changing the decay time t is straightforward in this approach and enables a direct calculation of the isotope specific inventory over time. Monte-Carlo approaches such as the freely available GEANT4 from CERN (geant4.web.cern.ch), FLUKA (www.fluka.org), or MCNP6 (laws.lanl.gov/vhosts/mcnp.lanl.gov) of the large-scale beam-matter interaction have their strength on particle transport and interactions in complex geometries. Whenever time dependence is of minor importance, for example in shielding calculations, detector sensitivity studies, or planning of medical irradiations, the Monte-Carlo approach reveals its strength in geometrical calculations.

These large-scale codes include vast amount of physics coupling all possible radiation fields (photons, ions, neutrons, electrons), but in particular for analytical applications the physics of these code packages remains too general. These applications require specific codes including only the physics and technical aspects relevant to a single task, while trying to maintain a certain level of productivity in the form of device control, data frameworks, user interfaces, and computational speed. Atomic scale effects such as displacement damage, collision cascades, and surface sputtering exploiting the Monte-Carlo approach in the so-called binary collision approximation are SRIM (srim.org) and SDtrim.SP (www2.ipp.mpg.de/~stel/SDTrimSP.html). Analysis codes for analytical methods integrate specific material models with differences connected to the sensitivity of the corresponding method. The small angle X-ray scattering code SASfit (sourceforge.net/projects/sasfit) for example includes >200 structural models with physical relevance and separable impact on the scattering spectra in connection with a fitting algorithm adapted to consider the relevant parts of the spectra. The MeV ion-beam analysis codes SimNRA (Mayer, SimNRA User's Guide IPP Report Number: IPP 9/113, 1997) and NDF (www.surrey.ac.uk/ion-beam-centre/research-areas/ion-beam-analysis) on the other hand apply a layered sample structure with elemental concentrations individual to each layer, since the method features a depth resolution with elemental sensitivity. For methods with industrial maturity such as electron induced X-ray emission (a.k.a. energy-dispersive X-ray spectroscopy) instrument manufacturers provide their own codes.

All of these codes and packages represent application specific compendia selected and optimized for a more or less specific task. Adding a source term to the equation system or simulating a nuclear reaction spectrum or whatever these code packages do relies on codes describing the basic physics of ion-matter interactions. This chapter demonstrated the complex physics behind beam-matter interactions, namely stopping, reactions/interactions, and kinematics. Starting already at the stopping power complex physics and numerous experimental data have to come together. For this topic several codes exist such as A-star and P-star for protons and α-particles and

e-star for electrons (National Institute of Standards and Technology 2019). The most common code for arbitrary ions is the program SRIM(Ziegler et al. 2008) with the latest version of 2013 being available freely on www.srim.org. SRIM allows also for integration in user programs with the help of its sr.module outputing stopping powers if given projectile and target properties. The SRIM software features a large set of examples and input data comparisons proving its accuracy in the few percent range down to a few keV/amu. For electrons the program CASP (http://www.casp-program.org/) provides stopping powers, while CASINO (http://www.gel.usherbrooke.ca/casino) already extends beyond pure stopping and straggling. The Nucleonica database (Nucleonica GmbH 2014) provides a compendium of codes for electrons, ions, and also positrons and muons.

Calculation of nuclear reaction cross-sections remains a major challenge to date. It has to be distinguished between ab initio codes calculating the nuclei on the quark level and nuclear model codes based on a semi-empirical approach. The former include extreme amounts of interactions, since all quarks of a nucleus interact with all other quarks and gluons via the physics of quantum chromodynamics (QCD). These ab initio codes do not require input other than fundamental physical constants. Unfortunately, current computational technology limits the capabilities of QCD calculations rendering it currently irrelevant for the complicated resonance cross-sections of elements such as lithium and beyond. In contrast, nuclear model codes allow for calculating reaction cross-sections for any projectile-target combinations, but they require input about the structure of the involved nuclei and physical models of the involved interactions. These structural data include experimentally determined energy level schemes and state lifetimes peppered with the typical experimental limits and accuracies. The most famous codes are Talys (www.talys.eu) and EMPIRE (www.nds.iaea.org/empire). The Talys code supplies the TENDL database, often cited here, which contains total and differential cross-sections for nearly all possible reactions.

Many of the above mentioned software packages do not feature full graphical user interfaces (GUIs), but rather rely on a scripting language for user input. Programming becomes a central skill of a least higher level accelerator application experts and researchers. This relates not only to the operation of codes, but also post-processing of data such as fitting and extraction of results. The simple adjustment of a beam position requires only three points for a skilled operator able to apply a polynomial fit of 2nd grade to the data, while the simple non-programming skilled approach might require acquiring a dozen data points, stepwise approaching a minimum value. Programming or data science, respectively, nowadays often termed artificial intelligence “AI” in business presentations, becomes the accelerator experts sixth sense. The author recommends to any reader from personal experience to acquire solid programming skills when working in this field. Even human resources departments value the programming skills of accelerator physicists due to this natural connection. The programming language Python has proven to be maybe the most valuable option in the recent years. Not only is the syntax quite flexible and straightforward and its whole is based on open source, but most importantly it features numerous packages

with pre-programmed complex functions for mathematics, data handling, and so on. Some of the graphs presented in this book also found on Python codes.

```
import numpy as np
from scipy.interpolate import interp1d
import scipy.integrate as integrate
import matplotlib.pyplot as plt

def integral(z):    # generate a function for integration
    x = np.genfromtxt("C:/pn cross-sec.txt", delimiter='\t', skip_header=1, usecols=0)
    y = np.genfromtxt("C:/pn cross-sec.txt", delimiter='\t', skip_header=1, usecols=1)

    xs  = np.genfromtxt("C:/p stopping h2o.txt", delimiter='\t', skip_header=1, usecols=0)
    stop= np.genfromtxt("C:/p stopping h2o.txt", delimiter='\t', skip_header=1, usecols=1)

    fsig = interp1d(x, y)
    fstop = interp1d(xs, stop)
    return integrate.quad(lambda x: fsig(x)/fstop(x), 1, z, limit=5000)

def integralOverE(z):    # generate a function with normalisation
    x = np.genfromtxt("C:/pn cross-sec.txt", delimiter='\t', skip_header=1, usecols=0)
    y = np.genfromtxt("C:/pn cross-sec.txt", delimiter='\t', skip_header=1, usecols=1)
    xs  = np.genfromtxt("C:/p stopping h2o.txt", delimiter='\t', skip_header=1, usecols=0)
    stop= np.genfromtxt("C:/p stopping h2o.txt", delimiter='\t', skip_header=1, usecols=1)

    fsig = interp1d(x, y)
    fstop = interp1d(xs, stop)
    return (integrate.quad(lambda x: (fsig(x)/fstop(x)), 1, z, limit=5000)/z)

xnew = np.linspace(1, 60, num=60, endpoint=True)
Integ= np.array([integral(xi)[0] for xi in xnew])    #slow but ok, thats not the problem
IntegE= np.array([integralOverE(xi)[0] for xi in xnew])    #slow but ok, thats not the problem

plt.plot(xnew, IntegE*10, 'o', xnew, Integ, '-')
plt.legend(["H x10", 'W'], loc='best')
plt.show()
```

The above code generates Fig. 3.18 from two files containing plain text lists of discrete points of the corresponding projectile energy dependent reaction cross-section and stopping power. The program interpolates these discrete lists forming integrable functions. The integrals are evaluated in a range of 1–60 MeV and plotted. Packages such as SciPy (Jones et al. 2001) and Numpy (Walt et al. 2011) ease this task by providing ready to use functions for most mathematical tasks. Packages for the export and complex plotting of the data exist allowing for fully automated parameter studies and acceleration of repeated analysis tasks. Even nuclear data packages exist for python integration.

References

G. Audi, et al., The NUBASE2016 evaluation of nuclear properties. Chin. Phys. C **41**, 030001, S (2017). https://doi.org/10.1088/1674-1137/41/3/030001

M. Berger, J. Hubbell, S. Seltzer, J. Chang, J. Coursey, R. Sukumar, D.S. Zucker, K. Olsen, *NIST XCOM: Photon Cross Sections Database* (Von abgerufen, 2010). https://www.nist.gov/pml/xcom-photon-cross-sections-database (2010)

J. Blocki, J. Randrup, W. Swiatecki, C. Tsang, Proximity forces. Ann. Phys. **105**, 427–462, S. (1977). https://doi.org/10.1016/0003-4916(77)90249-4

G. Ciullo, R. Engels, M. Büscher, A. Vasilyev, *Nuclear Fusion with Polarized Fuel* (Springer 2016)
Culham Centre for Fusion Energy, *FISPACT-II Material Handbooks*. (Abgerufen am 05 2018 von, 2018). https://www.ccfe.ac.uk/fispact_handbooks.aspx
A.F. Gurbich, SigmaCalc recent development and present status of the evaluated cross-sections for IBA. Nucl. Instrum. Methods Phys. Res., Sect. B **371**, 27–32 (2016). https://doi.org/10.1016/j.nimb.2015.09.035
M. Herman, R. Capote, B. Carlson, P. Oblozinsky, M. Sin, A. Trkov, V. Zerkin, EMPIRE: nuclear reaction model code system for data evaluation. Nucl. Data Sheets **108**, 2655–2715 (2007)
W. Huang et al., The AME2016 atomic mass evaluation (I). Evaluation of input data; and adjustment procedures. Chin. Phys. C **41** 030002, S (2017). https://doi.org/10.1088/1674-1137/41/3/030002
E. Jones, E. Oliphant, P. Peterson, et al., *SciPy: Open Source Scientific Tools for Python* (Von abgerufen, 2001). http://www.scipy.org/
A. Koning, et al., *TENDL-2015: TALYS-Based Evaluated Nuclear Data Library* (Von abgerufen, 2015). https://tendl.web.psi.ch/tendl_2015/tendl2015.html
M. Mayer, *SimNRA User's Guide IPP Report Number: IPP 9/113* (Max-Planck-Institut für Plasmaphysik, Garching). www.simnra.com
S. Möller, Analytical continuous slowing down model for nuclear reaction cross-section measurements by exploitation of stopping for projectile energy scanning and results for 13C(3He,α)12C and 13C(3He,p)15N. Nucl. Instrum. Methods Phys. Res. Sect. B **394**, 134–140 (2017). https://doi.org/10.1016/j.nimb.2017.01.017
National Institute of Standards and Technology, *NIST: Introduction of e-star, p-star, and a-star*. (Von abgerufen, 2019). https://physics.nist.gov/PhysRefData/Star/Text/intro.html
M. Nastasi, J.W. Mayer, Y. Wang, *Ion Beam Analysis: Fundamentals and Applications.* CRC Press (2014)
Nucleonica GmbH., *Nucleonica Nuclear Science Portal*. (www.nucleonica.com) *Version 3.0.49* (Nucleonica GmbH Karlsruhe, Germany, 2014)
OECD Nuclear Energy Agency (NEA), *JANIS* (Von abgerufen, 2017). http://www.oecd-nea.org/janis/
P. Sigmund, *Particle Penetration and Radiation Effects: General Aspects and Stopping of Swift Point Charges* (Springer, Berlin, Heidelberg, New York, 2006). ISBN 13978-3-540-31713-5
J. Sillanpää, Electronic stopping of silicon from a 3D charge distribution. Nuclear Instrum. Methods Phys. Res. Sect. B: Beam Interact. Mater. Atoms Vol. **164–165**, 302–309 (2000)
S.V. Walt, Colbert, S. C., G. Varoquaux, The NumPy array: a structure for efficient numerical computation. Comput. Sci. Eng. **13**, S. 22–30 (2011). https://doi.org/10.1109/mcse.2011.37.a
V. Zagrebaev, A. Denikin, A. Karpov, A. Alekseev, M. Naumenko, V. Rachkov, M.A. Naumenko, V. Saiko, *NRV Web Knowledge Base on Low-Energy Nuclear Physics—2 Body Kinematics* (Von abgerufen, 2019). http://nrv.jinr.ru/nrv/mobilenrv/kinematics/Kinematics2Body.html
J.F. Ziegler, J.P. Biersack, M.D. Ziegler, *SRIM—The Stopping and Range of Ions in Matter* (Chester, 2008)